Temp #181196

Relay I Trapped Radiation Measurements

by

C. E. McIlwain, R. W. Fillius*, J. Valerio, and A. Davé

March 1964

Department of Physics

University of California at San Diego

La Jolla, California

* visiting from the State University of Iowa, Iowa City, Iowa

Relay I Trapped Radiation Measurements

by

C. E. McIlwain, R. W. Fillius*, J. Valerio, and A. Davé

March 1964

Department of Physics

University of California at San Diego

La Jolla, California

Supported by NAS 5-1683
and NAS R-116

*visiting from the State University of Iowa, Iowa City, Iowa

ABSTRACT

33123

Instruments aboard the Relay I satellite have measured the intensities of geomagnetically trapped electrons with energies greater than 0.45 Mev and of protons in four energy ranges between one and 60 Mev over the region between 1.2 and 2.3 earth radii during the year 1963. The equatorial intensity of electrons ($E > 0.45$ Mev) was found to decrease monotonically from a maximum intensity of about 0.7×10^8 at 1.3 earth radii down to 10^5 $sec^{-1}cm^{-2}ster^{-1}$ at 2.3 earth radii. The principal maximum in the proton intensities was found to occur on consistently higher lines of force and with increasing intensities toward lower energies such that a maximum intensity of about 3×10^6 protons ($E > 1.1$ Mev) $sec^{-1}cm^{-2}ster^{-1}$ occur at about 2.3 earth radii compared with the maximum of 1.95×10^3 protons ($E = 40$ to 110 Mev) $sec^{-1}cm^{-2}ster^{-1}$ at 1.5 earth radii. A large decrease in the proton intensities at L values greater than 2.2 earth radii occurred during the magnetic storm of September 22-23, 1963.

Arthur

TABLE OF CONTENTS

Part I

Description of Experimental Techniques

Introduction

A set of four particle radiation detectors was designed and constructed at the State University of Iowa (R. W. Fillius, 1963; D. C. Enemark, 1962) for flight aboard the Relay satellite. As was originally planned, the reduction and analysis of the data resulting from the successful launchings of the Relay I and Relay II satellites is now being performed at the University of California at San Diego. The present paper is based upon a partial analysis of the data obtained by Relay I during its first year in orbit.

The Relay I satellite was launched on December 13, 1962 into an orbit with an apogee of 2.07 earth radii, a perigee of 1.21 earth radii and an inclination of 47.5 degrees. The precession of the orbit is such that the complete spatial distribution of trapped particles in the region $1.15 < R < 2.2$ earth radii and $\lambda < 60$ degrees (magnetic coordinates) can be obtained within a period of 140 days.

Radiation Detection System

The identification of particles as protons or electrons and the determination of their kinetic energy is accomplished by judicious choices of sensor (size and type), detector shielding, and by proper choice of the electronic discrimination levels.

All the detectors produce a quantity of charge related to the energy lost by the incident particle in the sensor. Two of the sensors are of the solid state type and two are scintillation crystals mounted on photomultiplier

tubes. In the solid state detectors, designated here as B and C, the charge produced at the output is linearly related to the energy lost by the particle in the sensor. The amplifier output of the scintillation detectors here designat as A and D, is also related to the particle energy lost in the sensor but not always linearly.

To avoid difficulties due to variations in the capacitance at the sensor output, the input amplifier was designed to respond to the charge generated by the sensors rather than the voltage. At the output of these amplifiers is present a voltage pulse related to the energy loss in the sensors. Since the energy loss as a function of the energy of the incident particles can be both measured and calculated, the energy spectrum analysis is reduced to a voltage pulse height analysis.

Other electronic blocks common to each detector are: a delay line inter-stage network to clip the pulses to a length of .25 μsec, a voltage post amplifier and voltage amplitude discriminators. The amplitude discriminators form the input circuits to pulse height analyzers for each detector. Since analyzers for each detector are somewhat different they will be described individually. Photographs of Detector A and the B-C-D detector complex are shown in Figures 1 and 2.

The B, C, and D detectors are directionally sensitive with the consequent need for the knowledge of magnetic field orientation for accurate intensity measurements. Detector A however is an omnidirectional detector whose response is independent of the field orientation.

The systems design is governed by the dynamics of trapped particles in the earth's magnetic field. The particles are constrained to travel in approximately helical paths about the lines of force. The angle α which the

particle velocity makes with respect to the field line varies with the magnitude of the magnetic field B along the field line according to the equation $\sin^2 \alpha = B/B_m$ where B_m refers to the point $\alpha = 90^\circ$. The angular distribution about the field line is almost always such that the peak intensity occurs in the plane perpendicular to the field line, i.e. at $\alpha = 90^\circ$. The magnetometer gating is arranged so that counts are accumulated only when the detectors are pointing perpendicular to the field line. The complete angular distribution at any point can be obtained by obtaining the dependence of the intensity at $\alpha = 90^\circ$ upon B_m and using the equation $\sin \alpha = B/B_m$ to transform this dependence upon B_m into the α dependence at the desired value of B.

Since the peak intensity occurs normal to the magnetic field lines it is only necessary to determine when the field component along the detector axis is zero and arrange to turn on the detectors for an interval during which the rate is relatively constant. Previous measurements at 920 km have shown the angular distribution to be symmetrical about the normal plane and the intensity to vary less than 10% over 10° on either side of the peak. At Relay I altitudes the variation is expected to be even less. From this then it is seen that if the detector are turned on about 10° ahead of the zero crossing of the field and turned off about 10° after zero crossing, a good measure of the peak intensity can be made.

Relay I spins at approximately 2.7 rev/sec in a known sense. The detector gating was achieved by placing an AC coupled flux gate magnetometer about 13° ahead of the detector axis in rotation. At zero AC field crossing along the magnetometer axis, a turn on signal is generated which allows the detectors to accumulate counts for the fixed interval of exactly 24 satellite clock pulses, after which the detectors are gated off. With the satellite

clock rate of 1152 pulse/sec the on time is 0.021 sec or about 19° of revolution.

When the spin axis of the satellite happens to be aligned with the field line and the detectors are always in the normal plane and no AC field variation is seen by the magnetometer. Whenever the AC field variation remains less than ± 4 milligauss for one second, a free running multivibrator (at the nominal spin rate) is started to operate the magnetometer gating circuitry and an identification bit is transmitted to indicate that it is in the special mode. The conditions necessary for this special mode have been met in flight but is a rare occurrance.

In addition to the magnetometer gating scheme a large amount of sub-commutation is needed for the radiation experiments because only seven accumulators are available for all the outputs. Whenever possible all of the outputs of a particular detector are examined at once to allow a direct measure of the particle intensity in each energy increment during the same time interval. The accumulators and data conditioning system are both in the encoder and are not an integral part of the radiation experiment. It can be seen from the overall block diagram (Figure 3) that the basic clock frequency (1152 cps) of the encoder and a subcommutator advance signal are provided by the encoder. The clock signal is gated on (not shown explicitly in Figure 3) at the same time the detector outputs are sampled and fed to an accumulator in the encoder to provide a direct measure of detector live time. Detectors E and F shown which are channeled through the same gating system are from a separate experiment performed by Bell Telephone Laboratories. They will not be discussed here.

The subcommutator advance signal from the encoder has a period of twelve seconds, two seconds in one state and ten seconds in the other. In the ten second state the accumulators are free to register counts each time the detector

outputs are gated on by the magnetometer signal; in the two second part the accumulators are read out. Signal M is the gate from the magnetometer circuitry. It is in one state for 24 clock pulses (about 0.021 sec) and in its complement state $\overline{M}$ for the rest of the period (about 0.179 sec) when it is used for a background measurement on B3, C3, D3, B4, C4, and D4 each at different sub-commutator cycles. The term "background" is used to designate the counts accumulated when the detectors are not looking at the peak intensity.

It should be noted that with the exception of detector A, all detector analyzer outputs are fed to the sub-commutator where they are switched to the accumulators one detector at a time. These accumulators are read out once a second while counting for ten seconds, then inhibited and read out twice, then reset for the next detector. By rejecting the data in which the two final readouts do not agree, the probability of an erroneous reading produced by transmission noise is reduced to a very small value (in practice, very few errors in over 10^5 readings have been discovered). Detector A is permanently connected through its driver to an accumulator which is read out every second but is never reset. Accumulator overflow is detected during data reduction. The remaining lines shown are information signal for transmission; viz.,

1. Two identification bits to indicate subcommutator position.
2. One identification bit for magnetometer gating circuit mode.
3. One analog channel, sampled once a second, which time shares on an equal basis between the sine wave output of the magnetometer and on an identification bit to indicate which of the alternate outputs of the analyzers is in use.
4. Two identification bits from the Bell Telephone Laboratories experiment.

The measurements of the magnetometer signal can be compared with the computed magnetic vector to derive the orientation of the satellite spin vector. Shortly after the launch of Relay I, the spin vector was ascertained in this manner to be within 4° of a declination equal to -69° and a right ascension of 125° on the celestial sphere. The magnetometer signal can also be analyzed to measure hydromagnetic waves with periods between 2 and 8 minutes provided their amplitude is greater than 100γ (10^{-3} gauss).

In the detailed discussion of the detector parameters which follows, it will be convenient to consider them in the order of increasing complexity associated with their energy analyzing system.

Detector A Characteristics

Detector A is primarily an omnidirectional 35 to 300 Mev proton detector but with some sensitivity to high energy electrons. The sensor is a 0.932 cm diameter sphere of National Radiac Sintilon plastic scintillator optically coupled to the phototube through a conical light pipe (see Figure 4). The sphere is at the center of the two concentric hemispherical aluminum domes with sufficient separation so that particles entering from different forward directions will see the same amount of shielding; viz, 1.30 g/cm^2. This shielding thickness stops all protons of energy less than 34 Mev and electrons less than 2.7 Mev. The detector protrudes about 2 cm from the surface of the satellite so that the entire forward hemisphere is unobstructed by further shielding. Analysis has shown that since the angular distribution of the trapped radiation is cylindrically symmetrical, the number of particles entering this front hemisphere is independent of the detector orientation.

One amplitude discriminator is placed at the amplifier output with pulse height setting corresponding to the integral energy spectrum end point of

Co^{60}. For the scintillator's size and type this setting represents an energy loss in the crystal of approximately 1.0 Mev since the most important photon physical process at this energy is Compton scattering. Consequently, the detector proton and electron thresholds are 34 Mev and 3.7 Mev. In the proton case it is evident that the shielding thickness is the dominant parameter for setting the energy threshold. For the electron threshold the electronic discriminator level must be known accurately also.

An experimental measurement of the proton energy threshold was performed on the University of Minnesota linear accelerator and was found to be 34 Mev to an accuracy better than 3%. Full efficiency is reached at 35 Mev. Direct electron threshold measurements could not be performed because of the lack of a monoenergetic high energy electron source.

Detector D Characteristics

Detector D is primarily a directional electron detector with some sensitivity to protons. The sensor is a cylinder of National Radiac Scintilon 0.254 cm diameter and 0.254 cm in height. It is optically coupled to the phototube through a glass disc (see Figure 5) to provide an additional 0.81 g/cm^2 of shielding in the backward direction. A minimum of $\sim$.07 g/cm^2 of platinum shields the crystal from the forward direction except for a circular entrance area of 0.37×10^{-2} cm^2. Particles entering the scintillator from the forward direction must penetrate 0.048 g/cm^2 of aluminum foil after passing through a 27° conical acceptance aperture. From the parameters of shielding and entrance area - solid-angle product alone the geometric factors, G, are listed.

G	Electrons	Protons
2.38×10^{-3} cm^2-ster	0.20 to 3.0 Mev	5.0 to 20 Mev
8.80×10^{-3} cm^2-ster	greater than 3.0 Mev	greater than 20 Mev

Several features of the above list should be explained. The transition between the two values for geometric factor occurs when the range of incident particles exceed the 1.07 g/cm^2 of platinum. For particles greater than this range the sensitive entrance area expands to the full diameter of the cylindrical scintillator. Fortunately, both electron and protons intensities fall rapidly with increasing energy in the trapped radiation allowing the use of G = 2.38×10^{-3} cm^2-ster alone to a high degree of accuracy.

Four amplitude discriminators are placed at the amplifier output, each providing a point on an integral pulse height spectrum of the detected particles. In view of the previous discussion about the geometric factor it is seen that to high accuracy the shielding serves to solely determine a lower energy cutoff for electrons and protons. The energy equivalent of the electronic discrimination level settings will just add to this low energy cutoff to provide integral energy output channels labelled D1, D2, D3, and D4.

	Energy loss required	Electrons	Efficiency	Protons	Efficiency
D1	.13	> 0.30 Mev	.7	> 5.1 Mev	1.0
D2	.28	> 0.45 Mev	.6	> 5.1 Mev	1.0
D3	.43	> 0.62 Mev	.45	> 5.2 Mev	1.0
D4	.64	> 0.82 Mev	.13	> 5.2 Mev	1.0

When the counting rate due to protons is important, the differences in the efficiencies for protons and electrons in the different channels can be used to separately determine the electron and proton fluxes.

The discrimination levels can be reproducibly set with a laboratory Sr^{90} electron source by noting the number of counts at each output and the count ratios of neighboring levels. Basic calibration of the energy thresholds and efficiencies were obtained using the Bell Telephone Laboratories 1 Mev accelerator. A graph of the efficiency vs. energy shown in Figure 6 serves to illustrate the manner in which the stated integral energy levels were chosen. Further calibrations were made with a fission beta spectrum at Los Alamos with the following results for the product, the efficiency (ϵ), and geometric factor.

Channel	$(\epsilon_G)_{fission}$
D1	1.46×10^{-3} cm^2-ster
D2	1.16×10^{-3}
D3	5.92×10^{-4}
D4	1.18×10^{-4}

Detector B Characteristics

Detector B is a single solid state diode (an Ortec surface barrier detector) designed to detect protons with nominal energy from one to 4.5 Mev with a high discrimination against the ambient electron flux. Insensitivity to electrons is achieved through

1. use of a thin sensor so that entering electrons cannot deposit much energy in it.
2. discrimination levels that are set much higher than the pulse amplitude typically produced by electron energy loss in the sensor, and

3. the previously mentioned 0.25 μsec pulse clipping to decrease the probability of pulse pile-up of many low energy events.

Brass shielding about the sensor confines the effective solid angle, for protons of less than 85 Mev, to a cone of ±15°. Details of the aperture construction are shown in Figure 7. Two thin annular discs serve as electron baffles to reduce the scattering of electrons into the detector. A nickel foil 1.2 mg/cm^2 thick is mounted on the inner baffle to shield the detector from light. The 6.5 mm^2 sensor area results in a geometric factor for the detector 0.015 cm^2-steradian.

The detector B electronic discrimination levels (B_α, B_β, B_γ, B_δ) are set at 0.87 Mev, 1.41 Mev, 2.10 Mev and 3.84 Mev respectively. Due to the small depletion depth (100 microns) of the detector a given discrimination level may be triggered both by a proton which stops in the active depth and a higher energy proton which penetrates it. Penetrating protons of still higher energy cannot deposit sufficient energy in the active depth to trigger the discrimination level. A given pulse height can therefore by produced by protons with either of two different energies. This characteristic of detector B is displayed in Figure 8 where the discrimination levels marked. Here it is clearly shown that although the output of the discriminators are integral in pulse height they represent different differential proton energy intervals. Further, level B_δ is set higher than any possible pulse height obtainable from protons received through the entrance aperture. It can be triggered only by heavier particles, such as alpha particles, or protons (greater than 85 Mev) penetrating the side of the shield and traversing the detector sideways. Level B_4 yields a crude measure of the omnidirectional background flux which penetrates the shield and can be used to place an upper limit upon the alpha particle flux.

Adjacent discrimination levels are placed in anti-coincidence (top of Figure 8) to yield four output channels labelled as B1, B2, B3, B4 with proton energy ranges

B1	1.1 to 1.6 Mev and 7.1 to 14 Mev
B2	1.6 to 2.25 Mev and 4.75 to 7.1 Mev
B3	2.25 to 4.74 Mev
B4	greater than 85 Mev background channel.

It can be seen that the overlapping energy intervals have been eliminated but an unambiguous identification of an energy spectrum still depends upon some prior knowledge of spectral shape or additional data such as is available from detector C. Calibrations of these ranges are based partly upon protons generated by the $d(He^3,p)\ He^4$ reaction on the Cockcroft-Walton accelerator at the State University of Iowa, shielding calculations, and the use of an accurately calibrated electronic pulser. Reaction produced protons are used to determine the detector bias voltage required for the desired depletion depth and to find the upper cutoff energy for penetrating protons in each channel. Lower cutoff energies for non-penetrating protons are based upon the discrimination levels set by a calibrated pulser with allowance for the proton energy loss in the light-tight foil.

Detector C Characteristics

Detector C is a two element proton telescope which classifies proton energies in three bands from 18.2 to 63 Mev. Directionality and solid angle are defined by two 1 cm^2 Lithium drift detectors separated a distance of 2 cm with their faces parallel and their sides rotated at 45° with respect to each

other. The resulting geometric factor is 0.216 cm^2-steradian.

High energy protons coming from the forward direction penetrate both detectors producing time coincident pulses. The rear detector, designated C2, performs the pulse height analysis on the penetrating part of the characteristic while the front detector serves to resolve the ambiguity in the double values characteristic of the rear detector. Characteristics for detectors C1 and C2 are given in Figure 9 with the placing of electronic discrimination levels shown. The block diagram at the top of the figure indicates the logical sorting of discriminator levels which combine to form analyzer outputs C1, C2, C3, and C4. Output C4 is different from the other outputs in that it represents the singles rate of pulse amplitudes between $C2_\alpha$ and $C2_\beta$ rather than time coincident pulses in the two detectors. Channel C4 is used as a background monitor to allow an estimate of the random coincidence rate. The resultant differential energy proton channels are

C1	18.2 to 25 Mev
C2	25 to 35 Mev
C3	35 to 63 Mev
C4	background

These results are shown succinctly by Figure 10 where the foreground locus represents the energies recorded by the output channels when a proton traverses C1 first and the background locus when C2 is traversed first.

Once again protons from the $d(He^3,p)He^4$ reactions were used to determine the front and back dead layers and the depletion depth for the two component sensors. Typical values were found to be 4.7 Mev, 13 Mev, and 7.25 Mev respectively. A final check of lower energy cutoffs for two of the output channels was performed with the 40 Mev linear accelerator at the University of

Minnesota. Counting rates from the three channels as a function of incident proton energy compared well with the expected values calculated from the measured detector parameters and discrimination levels.

Detector Radiation Damage

A comparison of the detector A and D measurements with results from similar detectors aboard Explorer XV indicates that the effective amplification of the Relay I scintillation detectors decreased by about a factor of 1.3 during the first month in flight. The data also indicates that smaller decreases occurred during the next two months. All of the data taken since May 1, 1963 however is consistent with the assumption that the effective detector gains remained stable to within 10%. The absolute discrimination levels used in this paper are probably not in error by more than 15% but comparison with the data from Relay II will provide a more accurate and trustworthy determination of the characteristics assumed by the Relay I detectors after May 1, 1963.

In the case of detector D, the change in characteristics can be directly attributed to radiation damage in that the glass disc upon which the scintillator is mounted can be darkened by a particle radiation dose comparable to that received in flight. This source of difficulty has been corrected in the detector D units to be flown in the future by replacing the glass with sapphire.

Two effects of radiation damage were observed on the B detector. First, the resistivity of the silicon increased so that the depletion depth increased. Knowing that this change occurred (by the appearance of large pulses) the necessary minor modifications in the interpretation of the data can be made with confidence. The second effect was that after 120 days in orbit, the size of the pulses began to decrease so that after 160 days in orbit the counting rates

from the B detector approached zero. The total number of protons reaching the sensitive element of the detector by this time was about $10^{12}/cm^2$ corresponding to a radiation dose of about 10^6 Rads. The solid angle subtended by the detector B aperture was reduced by a factor of 2.2 on the unit in Relay II so that a somewhat extended detector life is anticipated.

After one year in orbit the counting rates due to protons in detector C remain the same as on the day of launch. This indicates that the radiation damage to the two sensors in this detector has not been important.

Part II

Spatial Distributions of Particle Fluxes

Electron Distributions

The usual magnetic coordinates B and L (McIlwain, 1961) are used throughout this paper to organize the data received from different locations in space. The L value for a point in space is approximately equal to the maximum radial distance reached by the line of force going through the point and is given in units of earth radii. B is the scalar magnitude of the magnetic field at that location in units of gauss.

After the initial reduction of the telemetered information, the counting rates from all 19 channels of data are interpolated to a particular set of L values: 1.1, 1.15, 1.2, etc.

Only July 9, 1962 a high altitude nuclear explosion injected large numbers of energetic electrons into trapped orbits in the earth's magnetic field. Subsequent measurements (McIlwain, 1963) have shown that at least

until February 1963 these electrons constituted an important radiation hazard to spacecraft traversing certain regions of space. The Relay I data presented here show that this situation persisted throughout the year of 1963.

The flux of electrons with energies greater than 0.45 Mev can be uniquely obtained by subtracting the D4 channel, (Detector D, fourth discrimination level) from the D1 channel to remove the proton contribution to the D1 counting rate. The unidirectional intensity perpendicular to the line of force of electrons greater than 0.45 Mev obtained in this manner is shown in Figure 11 as a function of B for a set of lines of force with L values between 1.25 and 2.7 earth radii. The actual data points are shown for some of these lines of force to illustrate the distribution and scatter of the data points.

In the future, as more data is received, analytic fits to these data points will be made as a function of B and time for each line of force. This will make possible a normalization of the intensities to a reference time which will considerably reduce the scatter in the data. Analytic fits will also simplify the integration of the unidirectional intensities to obtain the angular distributions and the omnidirectional intensities. In lieu of actual integration, it is a useful fact that the omnidirectional intensity is almost always within a factor of 1.5 of six times the unidirectional intensity perpendicular to the line of force.

The plot of contours of constant intensity in B-L space shown in Figure 12 were derived from the same data shown in Figure 11. The ratio of intensities between adjacent contours is $10^{0.25} = 1.778$.

Comparing these results with the Explorer XV data, which was obtained between November 1, 1962 and February 1, 1963, it is found that the relative

spatial distributions given by the two sets of data are identical to within 30% in the region L = 1.3 to 1.6. The absolute intensities obtained from the Relay I measurements in this region may be as much as a factor two lower than the earlier Explorer XV results. Determination of the true time dependence must await comparison with the Relay II results but the present results indicate that the time constant for decrease in the intensities in this region is greater than one year. Since few reliable measurements of electrons greater than 0.5 Mev were made previous to the "Starfish" event, it is not yet possible to determine what part of the intensities are due to naturally occuring electrons.

The Relay I omnidirectional detector (detector A) is sensitive to electrons with energies greater than 3.5 Mev and protons with energies greater than 34 Mev. As mentioned previously, the effective gain suffered an initial decrease. By May 1, 1963 the gain reached a stable value approximately a factor of 1.5 lower than before launch. This caused the discrimination level to approach the largest pulse size which can be produced by an electron thereby reducing the efficiency for electrons to about one tenth of the initial value. Since there were no independent measurements of high energy electrons made between February 1 and May 1, 1963, it is possible that the measured decrease of a factor 10 in the electron counting rates may include a factor due to the change in the trapped electron intensities. The Relay II results, when available, can be used to recalibrate the Relay I detector and will therefore remove most of the present uncertainty.

It should be noted that most of the pulses produced by protons in the Relay I detector A remained far larger than the discrimination level. The efficiency for protons can therefore be accurately computed.

At L values greater than 3.0 earth radii, the counting rate due to protons is very small, thereby permitting good measurements of the high energy electrons in the outer zone. The analysis of the complex time and spatial dependences of the outer zone is not yet complete and will therefore be presented in a later paper.

At L values of less than 1.45, over 80% of the detector A counting rate is due to electrons. The observed counting rates along several lines of force in this region are shown in the upper part of Figure 13. The corresponding contours of constant counting rate in B-L space are shown in the left side of Figure 14. For comparison, the contours of constant intensity of electrons with energies greater than 5 Mev as measured by Explorer XV are shown in Figure 15. As expected, the contours are very similar in the region L = 1.25 to 1.5. In the region L < 1.25, there probably has been an appreciable decrease in the high energy electron intensities, but no Relay I data taken in this region after May 1, 1963 is available, so that the reality of this decrease cannot be demonstrated.

Proton Distributions

During the period May 1, to September 22 of 1963 over 80% of the detector A counting rates in the region L = 1.8 to 2.8 earth radii were probably due to protons. The efficiency for protons rises rapidly from near zero at 34 Mev and remains constant within a factor of 1.5 between 35 and 300 Mev. Since the flux of protons with energies greater than 300 Mev is relatively small in the region being considered, the detector A counting rates correspond to the total flux of protons with energies greater than 35 Mev. The weighted average value of the efficiency times the geometrical factor is

calculated to be 1/3 cm^2 with a probable error of less than 30%. The counting rates along lines of force in this region are shown in the lower part of Figure 13. The cosmic ray contribution has been removed by subtracting 0.6 counts per second. The corresponding contours of constant counting rates are shown in the right hand part of Figure 14. These contours are very similar to the contours of 40 to 110 Mev protons measured by Explorer XV (McIlwain, 1963). The differences are well explained by the spatial dependence of the proton energy spectrum as measured by the Relay I detector C.

Detector C measures the unidirectional flux of protons in three energy ranges between 18.2 and 63 Mev. The lower two channels C1 and C2 have electron efficiencies of very near zero. The third channel, C3, has a small (~.001) efficiency for electrons with energies greater than 3 Mev as well as an efficiency of near unity for protons with energies between 35 and 63 Mev. The flux of electrons with energies greater than 3 Mev in the region below L = 1.5 are as much as ten thousand times the flux of 35 to 63 Mev protons, therefore the C3 channel does not yield reliable measurements of protons in this region. In the region of L = 1.5 to 3.0 earth radii however, there is little if any interference due to electrons.

The contours of constant intensity of protons with energies between 18.2 and 35 Mev along lines of force as measured by channels C1 and C2 are shown in Figure 16. The radiation damage to solar cells shielded by .4 g/cm^2 of material on satellites which traverse the region between 1.5 and 2.5 earth radii is primarily due to protons in this energy range.

The electron counting rates in the D4 channel after May 1, 1963 were only about 5% of the electron counting rates in the D2 channel. Since the efficiency for protons in the two channels are very nearly the same, the difference between the D2 and D4 channels can be used to estimate the fraction

of the D4 counting rate which is due to electrons. Along lines of force between L = 1.8 and 2.6 this fraction is observed to be less than 20% so that the counting rate due to protons can be computed with a probable error of less than 10%. The unidirectional intensities of protons with energies greater than 5.2 Mev derived in this fashion are shown in Figures 17 and 18.

The sum of the B1, B2 and B3 channels yields the flux of protons with energies between 1.1 and 14 Mev with little if any unwanted effects due to electrons. The contours of constant undirectional intensities of these protons are shown in Figure 19. Data coverage was rather poor during the time period in which detector B was operating properly, therefore the intensities given in some parts of this figure may be in error by as much as a factor of two. It is expected that a more complete analysis of the available data will reduce the probable error to less than 20%. Radiation damage to unshielded solar cells on satellites which traverse the region around 2 earth radii is primarily due to these low energy protons.

A comparison of Figures 14, 16, 18, and 19 reveals that the spatial distributions of protons are quite different in the different energy ranges. The proton energy spectrum is a strong function of L and on some lines of force the spectrum varies importantly with B. For all energies along all lines of force, the maximum intensity occurs at the magnetic equator. These maximum intensities for four different energy ranges are shown as a function of L in Figure 20. The intensities in the 40 to 110 Mev energy range are derived from the Explorer XV data. Unfortunately the proton energy spectrum over the full range of 1.1 to 110 Mev cannot be adequately represented by any simple spectral form like a power law or exponential dependence on energy. No one parameter, such as the E_o previously suggested (McIlwain and Pizzella, 1963)

has been found with which the spatial dependence of the spectrum can be easily characterized.

Detailed energy spectra can be obtained by using all eight of the channels producing proton data (channels B1, B2, B3, D4, C1, C2, C3, and A). This analysis is not yet complete and will be presented in a future paper.

Magnetic Storm Effects

Between 2100 hours UT on September 22 and 0300 hours UT on September 23 the largest fluctuations in the earth's magnetic field during the year of 1963 occurred. Within almost the same short period of time, the proton distribution measured by detector A underwent a radical change. The new distribution of protons with energies greater than 35 Mev is shown in the right side of Figure 21. For comparison, the earlier distribution is shown on the left side. At L values of less than 2.0 no change larger than 10% was observed while outside L = 2.5 the intensities typically decreased by over a factor of ten. The earlier distribution had remained stable for many months. Similarly, the new distribution has remained unchanged as of the latest observations which were made late in December 1963.

It seems quite possible that a thorough analysis of this event will reveal the true character of the mechanisms which control the behavior of trapped protons.

Simultaneous with the proton changes, an intense new outer zone of electrons began to form with a peak intensity at L = 3.2 earth radii. In addition to the relatively energetic electrons in the outer zone, a high intensity of low energy (less than 0.7 Mev) electrons appeared in a wide region of space. Immediately after the event, the unidirectional intensity of electrons

with energies greater than 0.45 Mev at a radial distance of 2.0 earth radii was greater than 3×10^6 sec cm^{-2} $steradian^{-1}$ from L = 4.0 down to at least L = 2.0. Referring to Figure 12, the contour corresponding to $\log_{10}(j_\perp) = 6.5$ apparently moved outward by over two earth radii. Unfortunately very little data was taken from the Relay I radiation detectors after this event (except from detector A, which is on continuously) until December by which time the anomalous low energy electron intensities had undergone considerable decreases.

Part III

Integrated Fluxes Along the Relay I Orbit

Daily Integrals

The Explorer XV data has been used to construct a computer program (McIlwain, 1963) which can be used to determine the omnidirectional fluxes of three categories of particles which were present at arbitrary locations in space on January 1, 1963. This program has been used to obtain the total flux of these particles striking the Relay I satellite over 8 complete revolutions (1.02 days) for 40 different days distributed throughout 1963. An examination of these results reveals two important facts: (1) the total flux per day varies smoothly from day to day, (2) the total flux per day for each category of particles is a unique function of the latitude of perigee (assuming no change of particle intensities with time). The dependence of the daily fluxes of particles upon the latitude of perigee, shown in Figure 21, can therefore be used (along with the known variation of the latitude of perigee with time) to determine the daily fluxes as a function of time as is shown in Figure 22.

The relative differences in the curves are of course due to the different spatial distributions of the particles. It is interesting to note that the daily fluxes of protons with energies greater than 1.1 Mev would be peaked at the times at the daily fluxes 40 to 110 Mev protons are a minimum.

Data from a detector on the INJUN 3 (Valerio, to be published) indicates that the flux of 40 to 110 Mev protons did not vary importantly during the first eight months of 1963 and the Relay I data indicates that the daily fluxes of electrons were no more than a factor of three lower at the end of 1963 than at the time of the Explorer XV measurements.

Integrals Over One Year

The curves in Figure 22 have been integrated over the first year after the launch of Relay I. The resulting average fluxes per day were found to be:

(1) $(2.1\ ^{+.3}_{-.8}) \times 10^{12}$ electrons ($E > 0.5$ Mev) $cm^{-2}day^{-1}$

(2) $(3.6\ ^{+.4}_{-1.7}) \times 10^{10}$ electrons ($E > 5$ Mev) $cm^{-2}day^{-1}$

(3) $(1.07 \pm .15) \times 10^{8}$ protons (E = 40 to 110 Mev) $cm^{-2}day^{-1}$

where the error limits correspond to the sum of all possible errors and the maximum possible changes in the particle intensities allowed by the Relay I measurements.

Since the solar cells comprising the Relay I power plant were shielded by about 0.4 g/cm^2 of quartz, which can be penetrated by protons with energies greater than about 17 Mev, it is of interest to anticipate the result of a proper integration of the data obtained by detector C. A comparison of the

bottom two curves of Figure 20 and similar curves for other latitudes leads to the estimate that the average flux of proton with energies greater than 18.2 Mev is a factor of 10 ± 2.5 larger than the average flux of 40 to 110 Mev protons. This flux of $(1.1 \pm .3) \times 10^9$ protons $(E > 18.2 \text{ Mev}) \text{cm}^{-2}\text{day}^{-1}$ appears to be adequate to produce the observed solar cell radiation damage (Waddel, private communication). For n-on-p type solar cells this average omnidirectional flux of protons produces radiation damage equivalent (Brown et al, 1963) to a beam of one Mev electrons at normal incidence with a flux of $(2.0 \pm .6) \times 10^{12}$ $\text{cm}^{-2}\text{day}^{-1}$. By comparison, the average electron spectrum implied by the data above, when weighted by the energy dependence of the electron damage to n-on-p type solar cells under 0.4 g/cm^2 of quartz (Brown et al, 1963) indicates that the average damage due to electrons was equivalent to a beam of only $(0.6 \pm .4) \times 10^{12}$ one Mev electrons $\text{cm}^{-2}\text{day}^{-1}$. These calculations therefore indicate that three quarters (.77 ± .17) of the damage to the solar cells protected by 0.4 g/cm^2 of quartz was probably produced by protons. The measured energy spectra of electrons and protons are such that as the shielding is reduced below 0.4 g/cm^2 the fraction of the damage produced by protons rapidly approaches unity.

Detector A is connected to a large register which is not reset after each reading and which accumulates $2^{29} \cong 5.37 \times 10^8$ counts before overflowing. The counts in this register can therefore be used to determine the total number of detector A counts per day. Some 300 measurements of this kind are shown in Figure 23. Since the detector was not designed to properly measure the high intensities of artificially injected electrons, the dead time corrections necessary are relatively large. The average correction factor for a day's accumulation of counts depends upon how the counts were obtained. For example,

a given number of counts obtained in a short time requires a larger correction factor than the same number of counts obtained in a longer period of time. The detailed rates of accumulation as predicted by the Explorer XV data has been used to calculate the desired average correction factor in a manner which is relatively independent of the variations in the detector A efficiency with time. The resulting calculated values for the true number of counts per day is shown in the upper curve of Figure 23. Except for the times where the number of counts per day exceeds 1.5×10^9, this curve is probably accurate to within 15%. For comparison, the computed intensity of electrons greater than 5 Mev (see Figure 22) multiplied by $0.02 \times \exp(-\text{day of year}/365)$ is shown in the bottom curve. After day 121 (May 1) it can be seen that the number of true counts per day was slowly decreasing but with a time constant of greater than one year. Since these daily counting rates are largely due to electrons it must be remembered that after May 1, the effective discrimination level was in a region of the electron pulse height distribution where a 2% change in discrimination level would produce a change in counting rate of at least 10% and probably about 20%. The apparent decrease in the daily number of counts can therefore be used only to indicate that there was no large change (i.e. larger than a factor of two) in the high energy electron fluxes between May 1 and December 10, 1963 and to indicate that the effective gain of the detector has been relatively stable since May 1, 1963.

Part IV

Summary of Results

The highest electron intensities are found around the magnetic equator at radial distances between 1.2 and 1.6 earth radii. The Relay I

data shows that intensities measured earlier in this region by Explorer XV persisted throughout the year of 1963 and did not decay by more than a factor of three.

The spatial distribution of protons in four different energy ranges has been determined and found to depend strongly upon energy. The proton intensities at L values greater than 2.0 earth radii were observed to decrease during a large magnetic storm. At all other times the protons fluxes exhibited no important changes with time.

The integrated fluxes of various particle types along the Relay I orbit have been computed and are found to be adequate to explain the observed degradation of solar cells.

Acknowledgements

We wish to thank all the NASA and RCA personnel for their contributions to this experiment. This research was supported in part by NASA contracts NAS5-1683 and NASr-116.

References

Brown, W. L., J. D. Gabbe, and W. Rosenzweig, Results of the Telstar radiation experiments, Bell Syst. Tech. J., 92, Nov. 4, part 2, 1505-1957, 1963.

Enemark, D.C., Electrical design of the radiation effects experiment for the satellite Relay, SUI 62-16 (State University of Iowa, Master's Thesis, 196

Fillius, R. W., Satellite instruments using solid state detectors, SUI 63-26 (State University of Iowa, Master's thesis, 1963).

McIlwain, C. E., Coordinates for mapping the distribution of magnetically trapped particles, J. Geophys. Res. 66, 3681-3691, 1961.

McIlwain, C. E. and G. Pizzella, On the energy spectrum of protons trapped in the earth's inner Van Allen zone, J. Geophys. Res. 68, 1811-1823, 1963.

McIlwain, C.E., The radiation belts, natural and artificial, Science, 142, 355-361, 1

Figure Captions

Figure 1. Photograph of the Relay I omnidirectional detector A.

Figure 2. Photograph of the Relay I B-C-D directional detector complex.

Figure 3. Overall block diagram of the radiation detector system including the Bell Telephone Laboratories detectors E and F. The satellite clock and subcommutator advance from the encoder serve as the input timing signals.

Figure 4. Detector A scintillator mount and shielding.

Figure 5. Detector D scintillator mount, shielding, and aperture.

Figure 6. Relative efficiency vs. energy curves for detector D outputs.

Figure 7. Detector B aperture.

Figure 8. Typical detector B energy response characteristic with discriminator settings indicated. Logical combinations of the discriminator levels to produce outputs are shown at the top of the figure.

Figure 9. Typical detector C energy response characteristics with discriminator settings indicated. The logical combinations of the six discrimination levels used to produce the outputs are shown at the top of the figure.

Figure 10. Two-dimensional view of detector C telescope proton energy analysis.

Figure 11. The unidirectional intensity perpendicular to the magnetic field of electrons with energies greater than 0.45 Mev as a function of B for various L values.

Figure 12. Contours of constant intensities derived from Figure 11. The contours are labelled by the logarithm to the base ten of the intensity. Four contours per decade are given corresponding to a factor of $10^{0.25} = 1.78$ in intensity between adjacent contours.

Figure 13. The counting rate of the omnidirectional detector (detector A) along various lines of force. Below L = 1.45 the observed counting rates are primarily due to electrons and above L = 1.7 the counting rates are primarily due to protons. The cosmic ray contribution has been removed by subtracting 0.6 counts/sec.

Figure 14. Contours of constant counting rate derived from Figure 13.

Figure 15. Contours of constant omnidirectional intensity of electrons with energies greater than 5 Mev derived from Explorer XV data.

Figure 16. Contours of constant unidirectional intensity of protons with energies between 18.2 and 35 Mev as derived from detector C data.

Figure 17. The unidirectional intensity of protons with energies greater than 5.2 Mev along lines of force as derived from detector D data.

Figure 18. Contours of constant intensity derived from Figure 17.

Figure 19. Contours of constant unidirectional intensity of protons with energies between 1.1 and 14 Mev as derived from detector B data.

Figure 20. Unidirectional intensities perpendicular to the magnetic field for four different proton energy ranges as a function of L along the magnetic equator.

Figure 21. Contours of constant detector A counting rates before and after the magnetic storm of September 22, 1963. Multiplication of the counting rates by three yields the omnidirectional flux per square centimeter of trapped protons with energies greater than 35 Mev.

Figure 22. Total omnidirectional fluxes of several categories of trapped integrated around the Relay I orbit as a function of the latitude of perigee based upon the January 1, 1963 distributions measured by Explorer XV.

Figure 23. Daily average omnidirectional intensities versus time for Relay I as derived from Figure 22.

Figure 24. The total counts per day registered by detector A. The data points correspond to the number of counts registered in the accumulator. The upper curve represents the same data after correction for the 3 microsecond detector dead time.

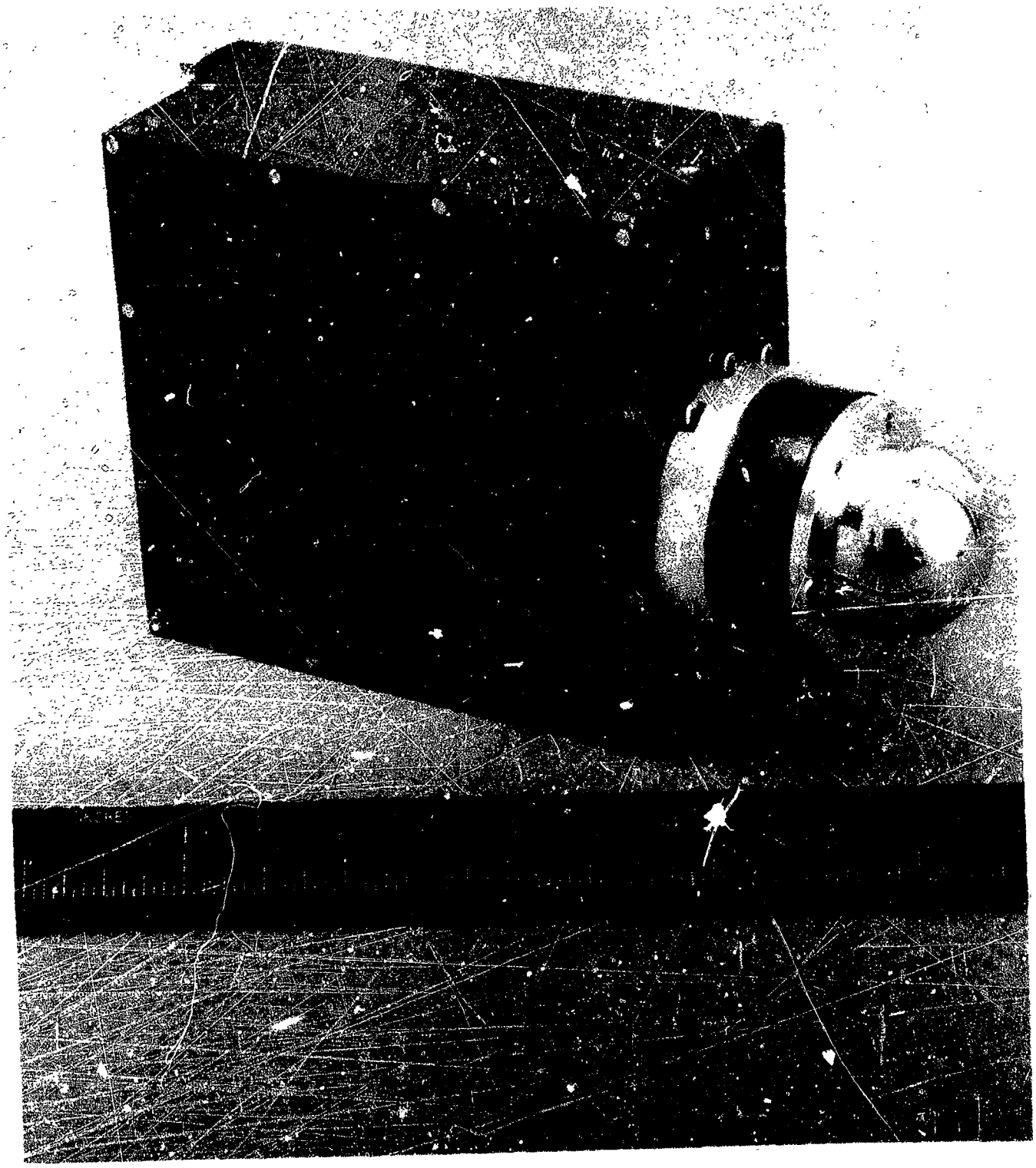

Figure 1

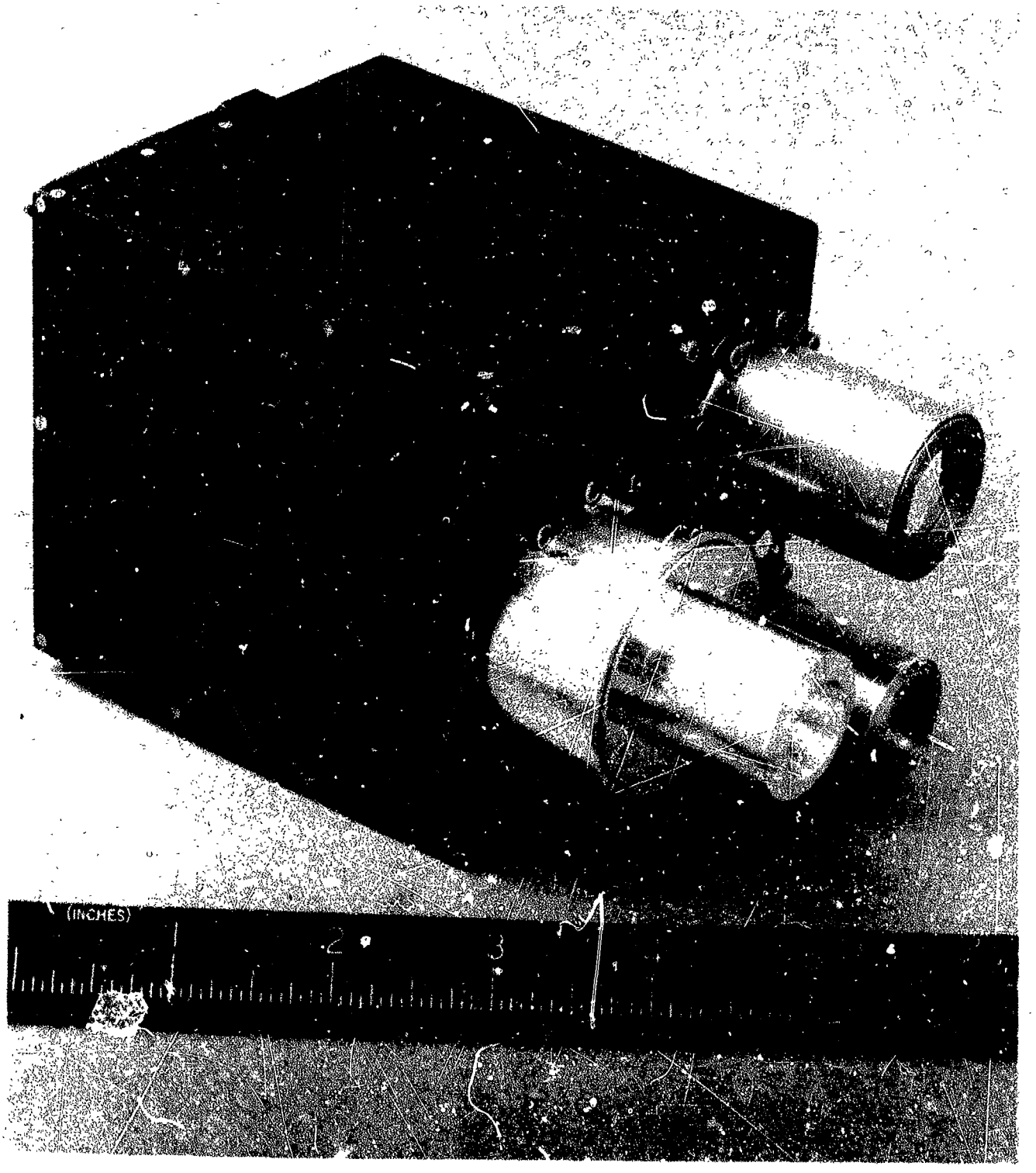

Figure 2

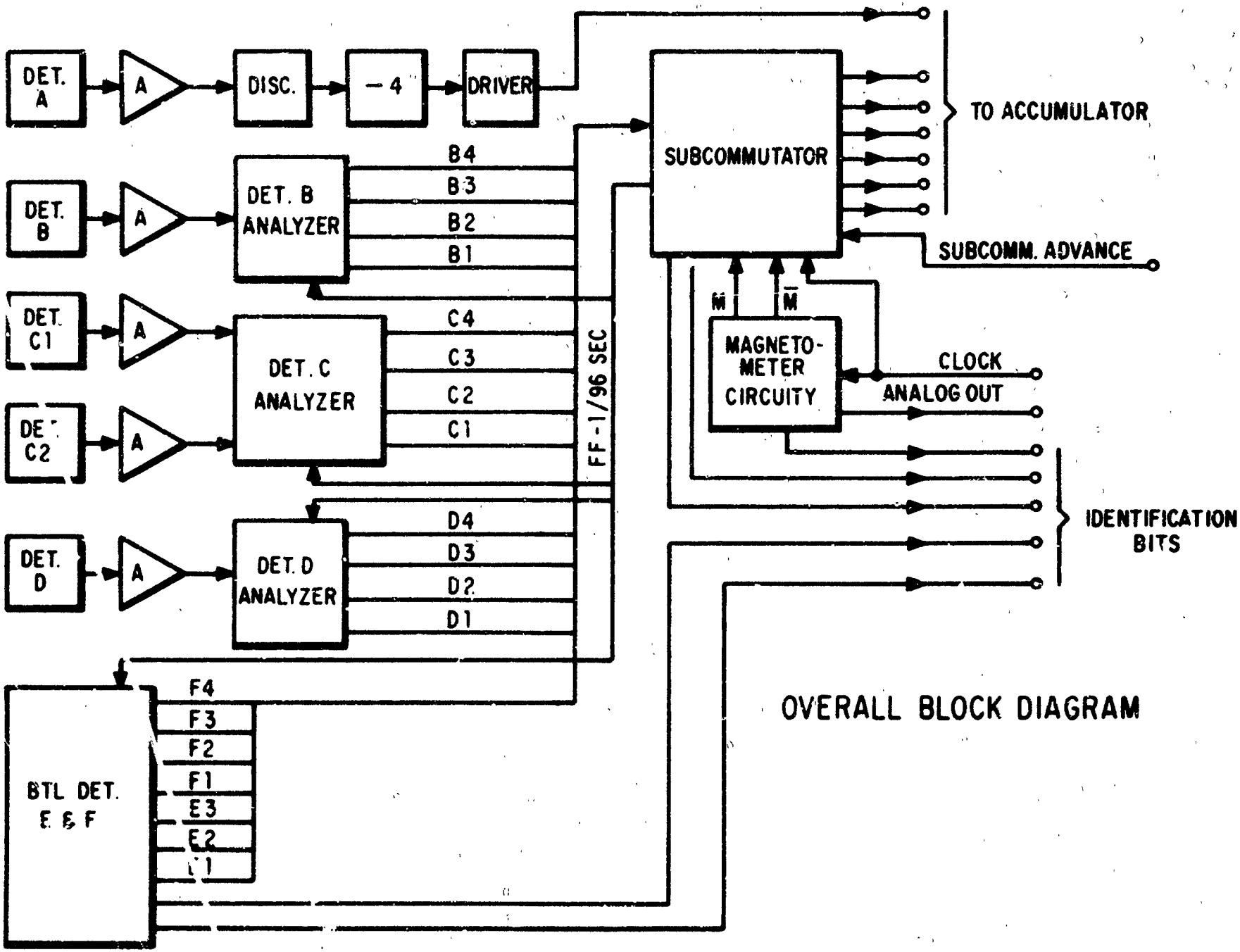

OVERALL BLOCK DIAGRAM

Figure 3

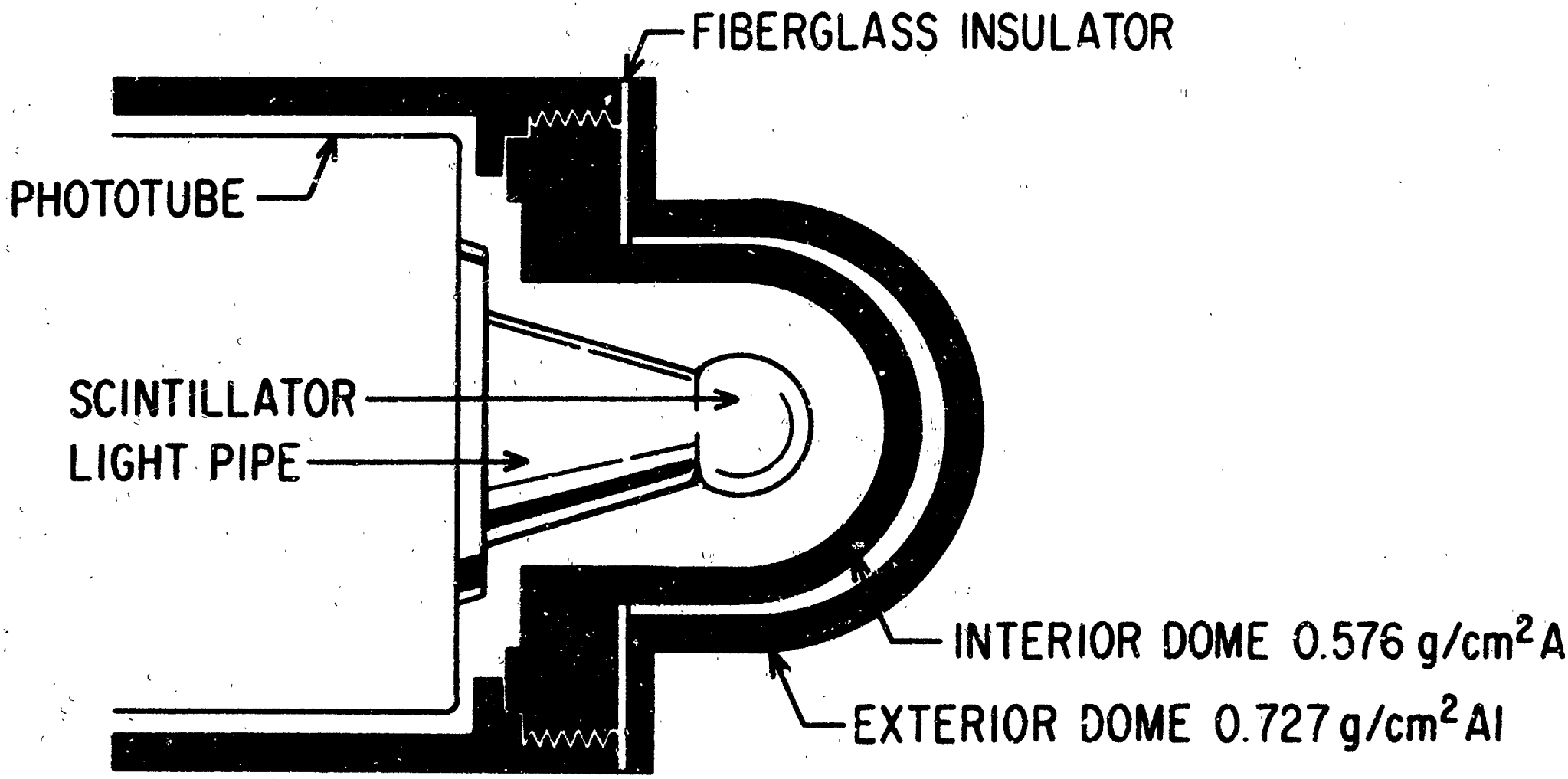

RELAY OMNIDIRECTIONAL DETECTOR

Figure 4

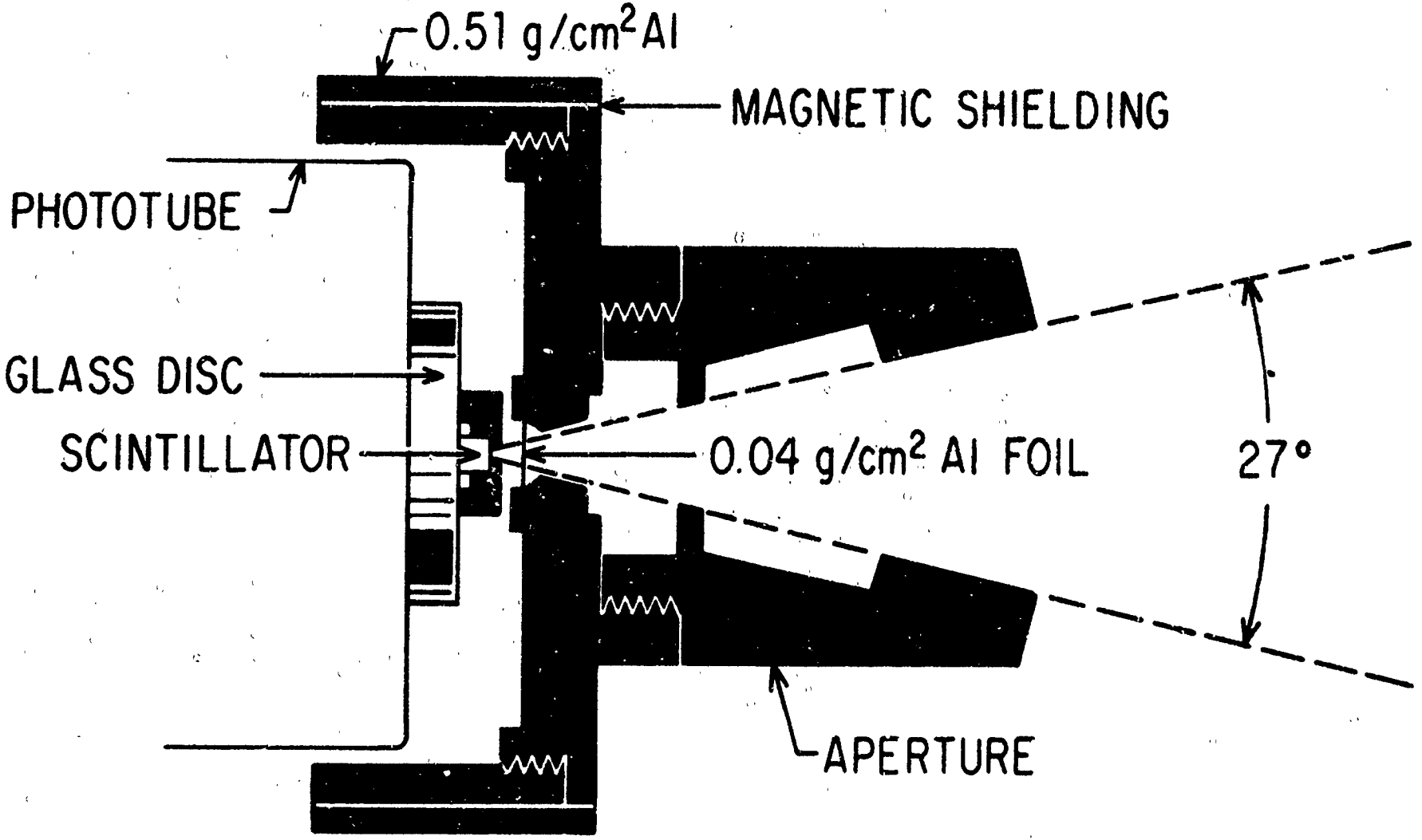

RELAY DIRECTIONAL DETECTOR

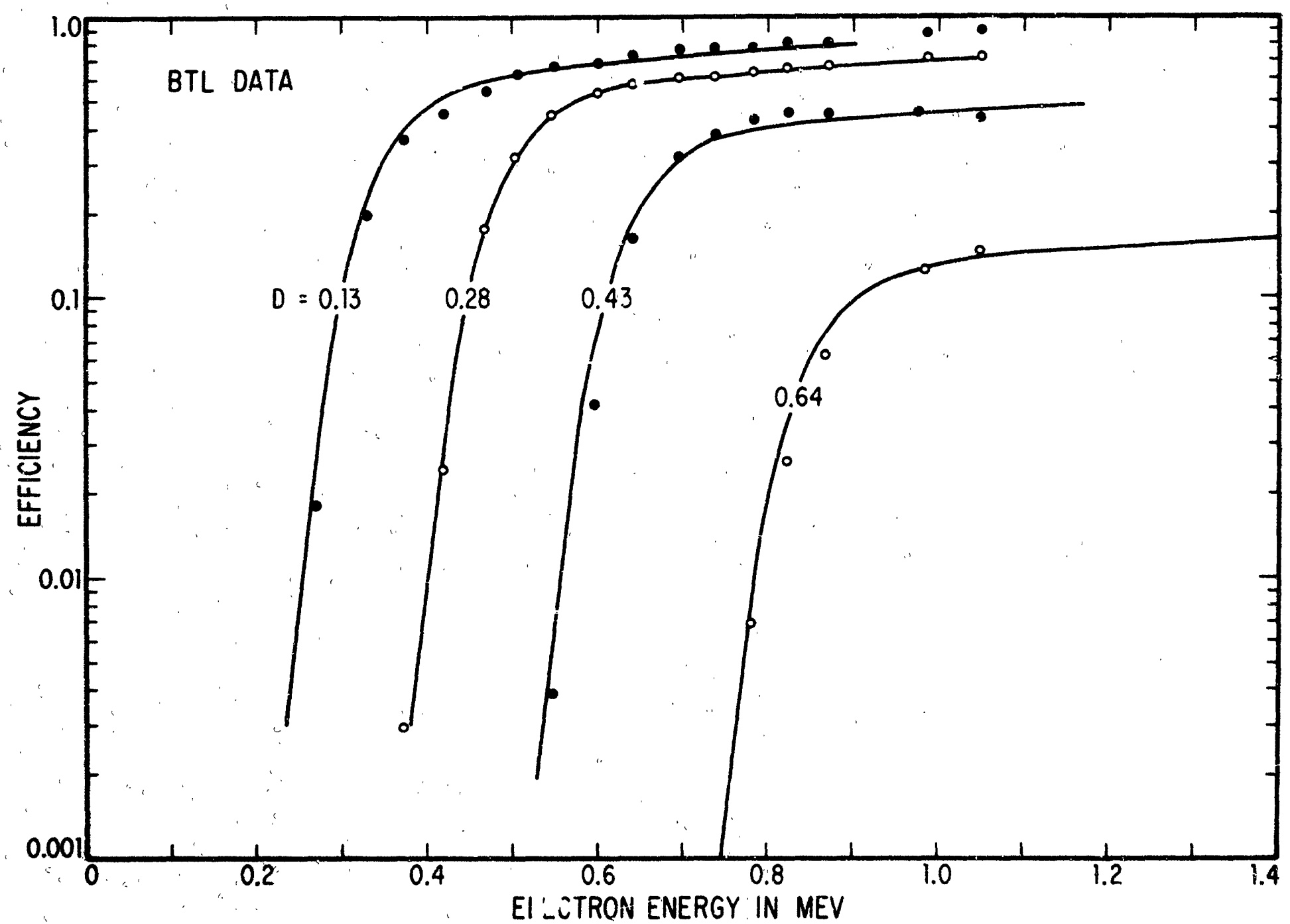
BTL DATA
D = 0.13
0.28
0.43
0.64
EFFICIENCY
1.0
0.1
0.01
0.001
0
0.2
0.4
0.6
0.8
1.0
1.2
1.4
ELECTRON ENERGY IN MEV

Figure 6

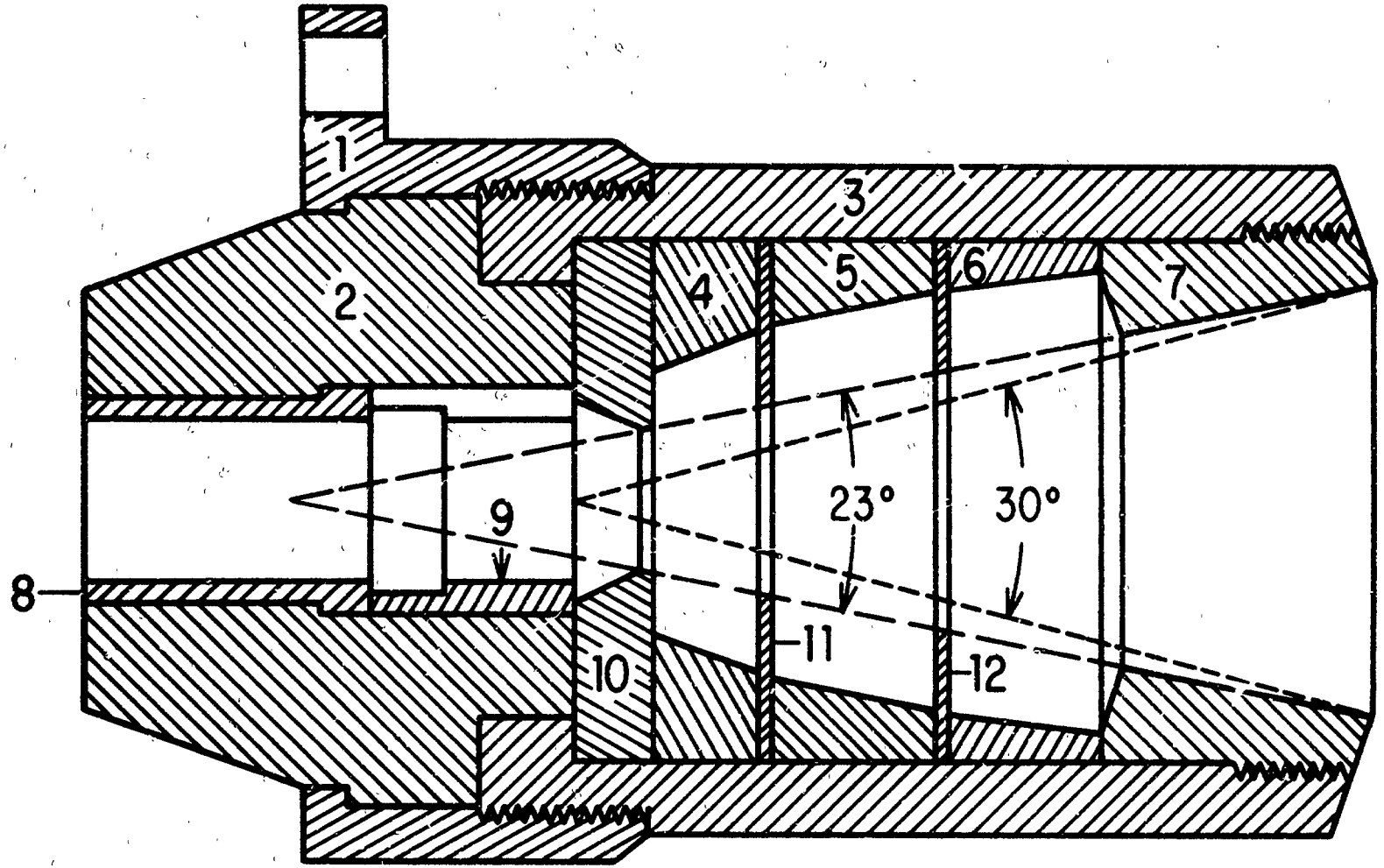

DETECTOR "B" APERTURE

1. MOUNTING RING
2. REAR SHIELD
3. MAIN HOUSING
4. REAR SPACER
5. SECOND SPACER
6. UPPER SPACER
7. APERTURE DEFINING
8. CONNECTOR INSULATOR
9. DETECTOR HOLDER
10. SOURCE MOUNT
11. ELECTRON BAFFLE
12. ELECTRON BAFFLE

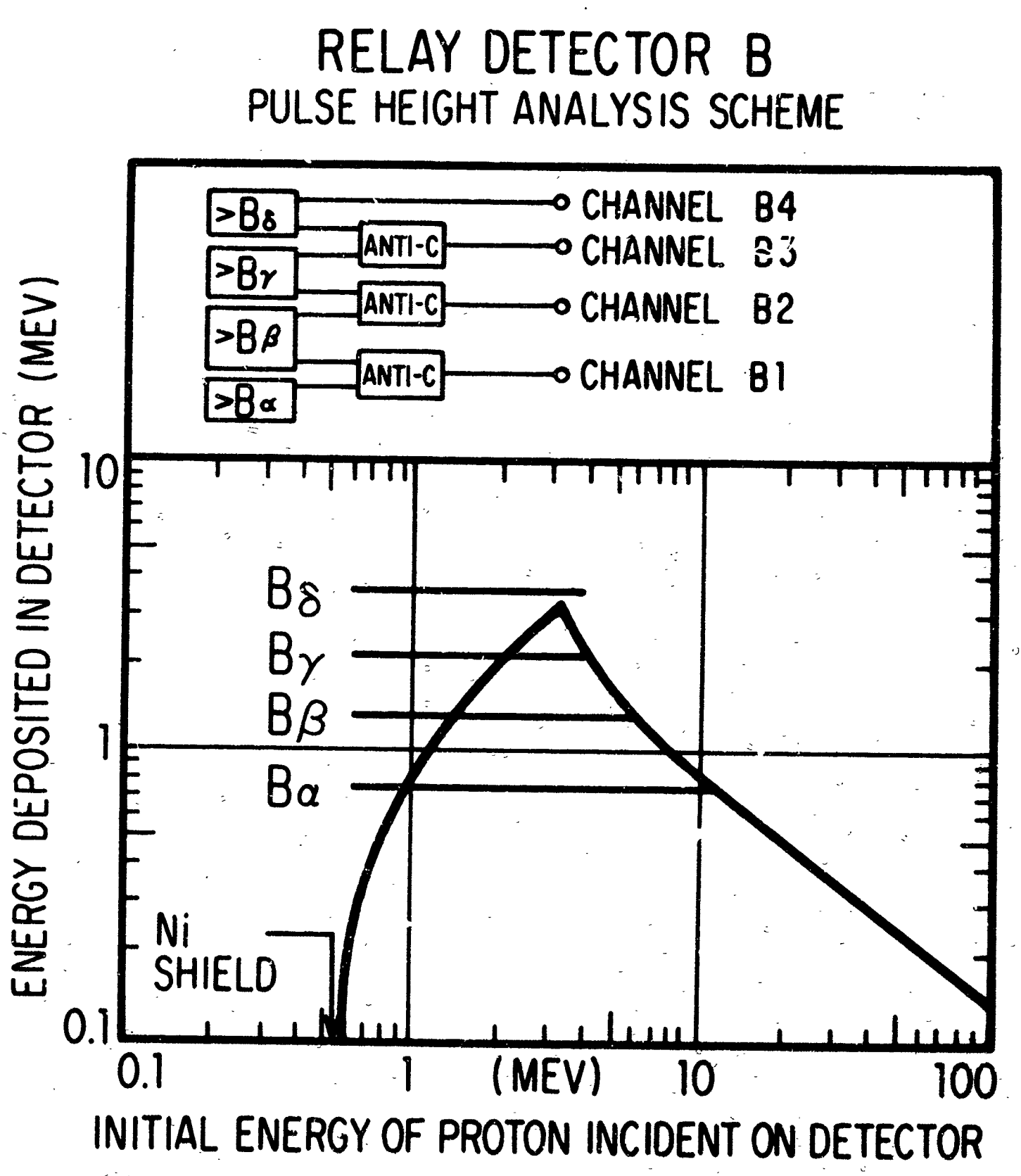
RELAY DETECTOR B
PULSE HEIGHT ANALYSIS SCHEME
>Bδ
>Bγ
>Bβ
>Bα
ANTI-C
ANTI-C
ANTI-C
CHANNEL B4
CHANNEL B3
CHANNEL B2
CHANNEL B1
Bδ
Bγ
Bβ
Bα
Ni
SHIELD
ENERGY DEPOSITED IN DETECTOR (MEV)
10
1
0.1
0.1
1
(MEV)
10
100
INITIAL ENERGY OF PROTON INCIDENT ON DETECTOR

Figure 8

TELESCOPE DETECTOR C PULSE-HEIGHT CHARACTERISTICS & BLOCK LOGIC

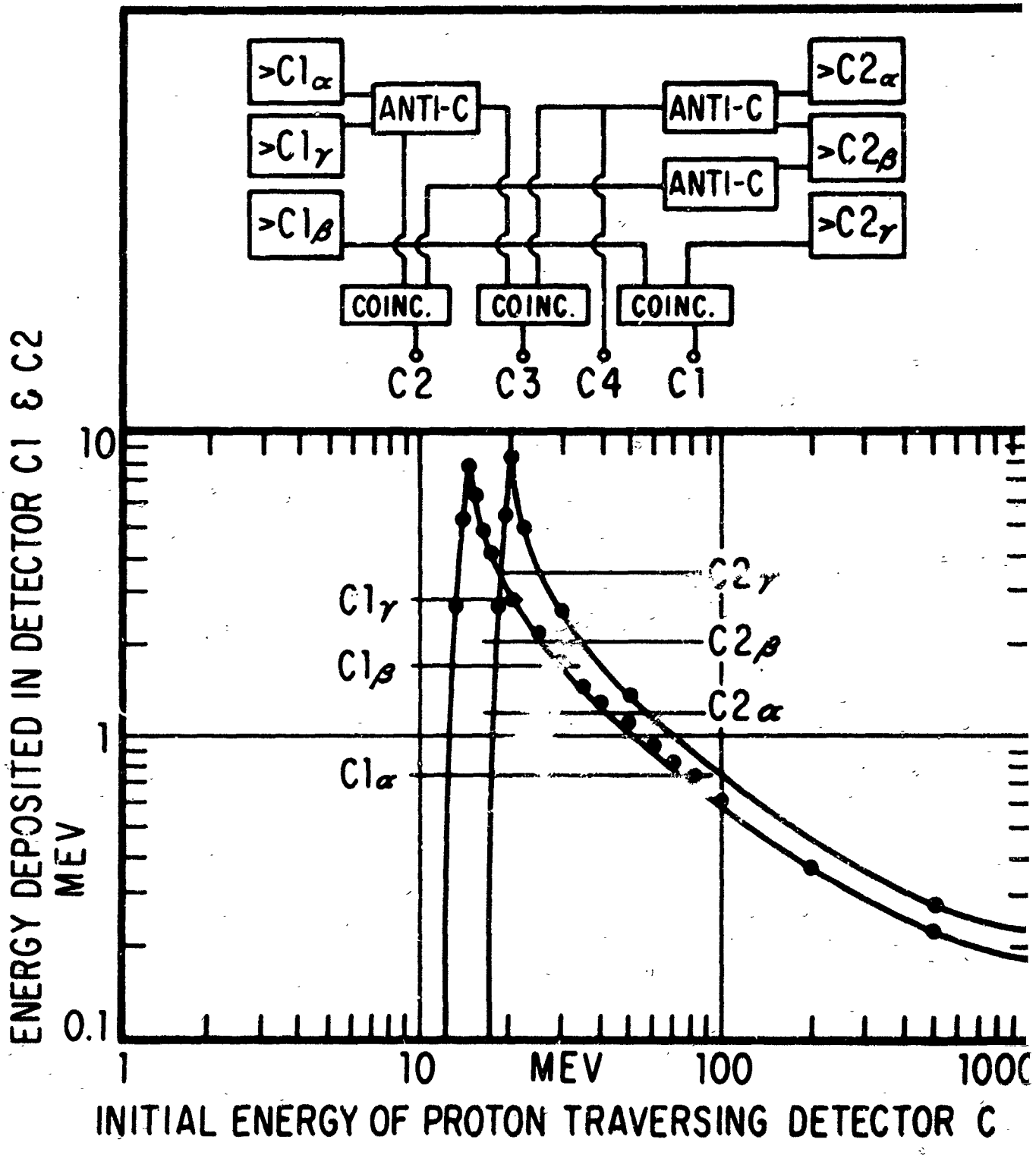

Figure 9

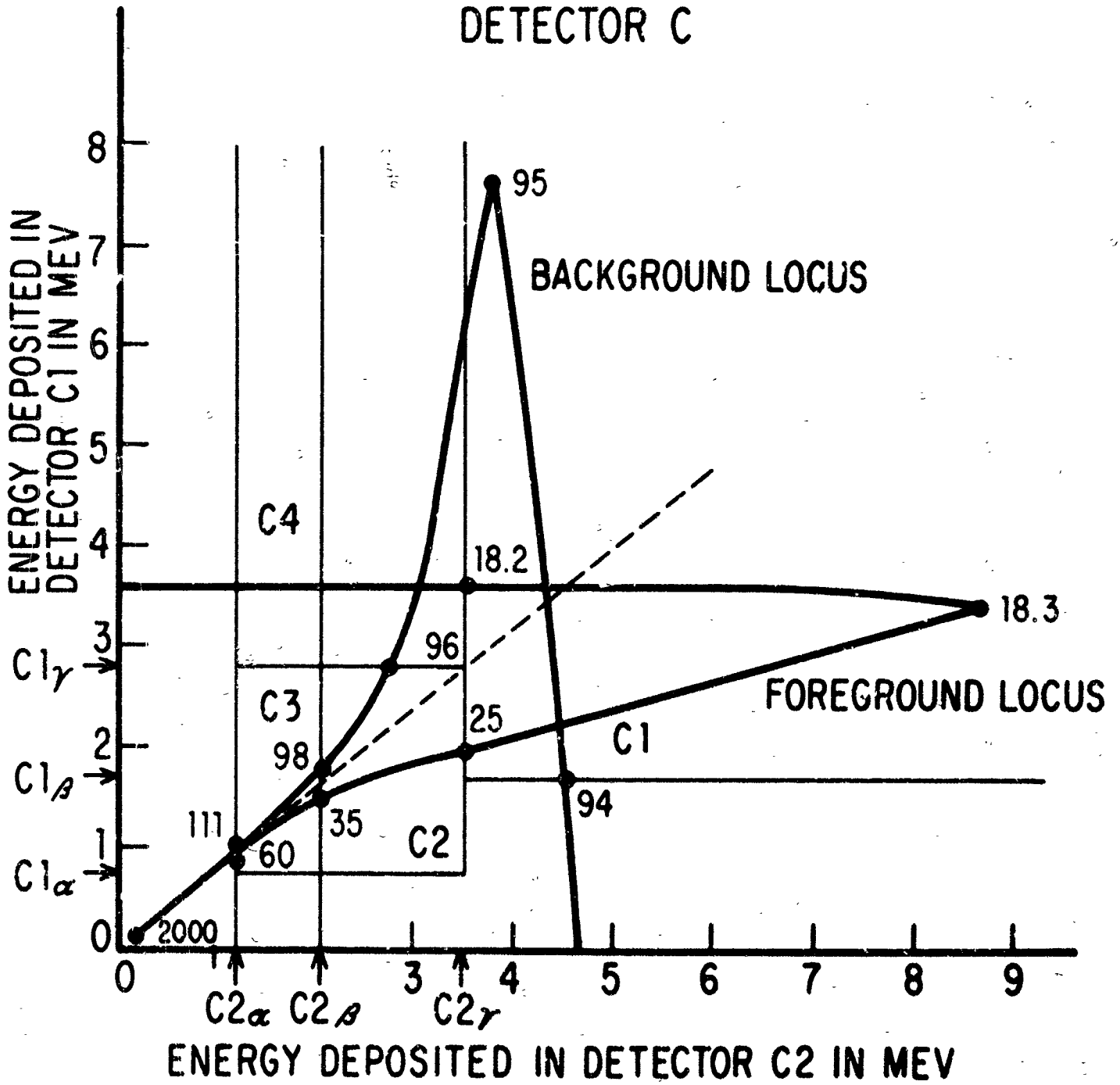
DETECTOR C
ENERGY DEPOSITED IN DETECTOR C1 IN MEV
BACKGROUND LOCUS
FOREGROUND LOCUS
C4
C3
C2
C1
95
18.2
18.3
96
25
98
94
111
35
60
2000
C1γ
C1β
C1α
C2α
C2β
C2γ
ENERGY DEPOSITED IN DETECTOR C2 IN MEV

Figure 10

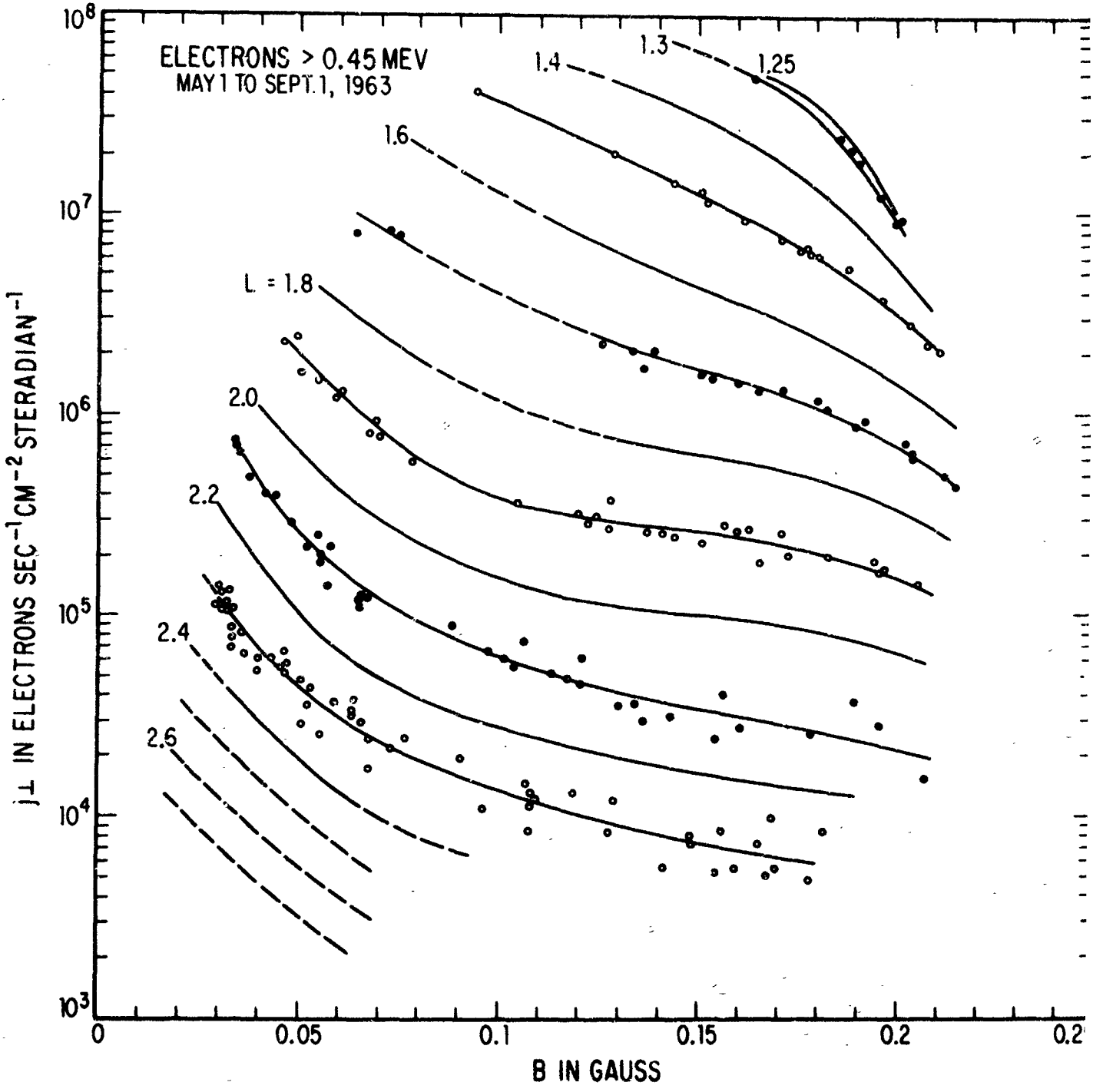
ELECTRONS > 0.45 MEV
MAY 1 TO SEPT. 1, 1963
1.3
1.4
1.25
1.6
L = 1.8
2.0
2.2
2.4
2.6
10^8
10^7
10^6
10^5
10^4
10^3
$j_\perp$ IN ELECTRONS $SEC^{-1} CM^{-2}$ STERADIAN^{-1}
0
0.05
0.1
0.15
0.2
B IN GAUSS

Figure 11

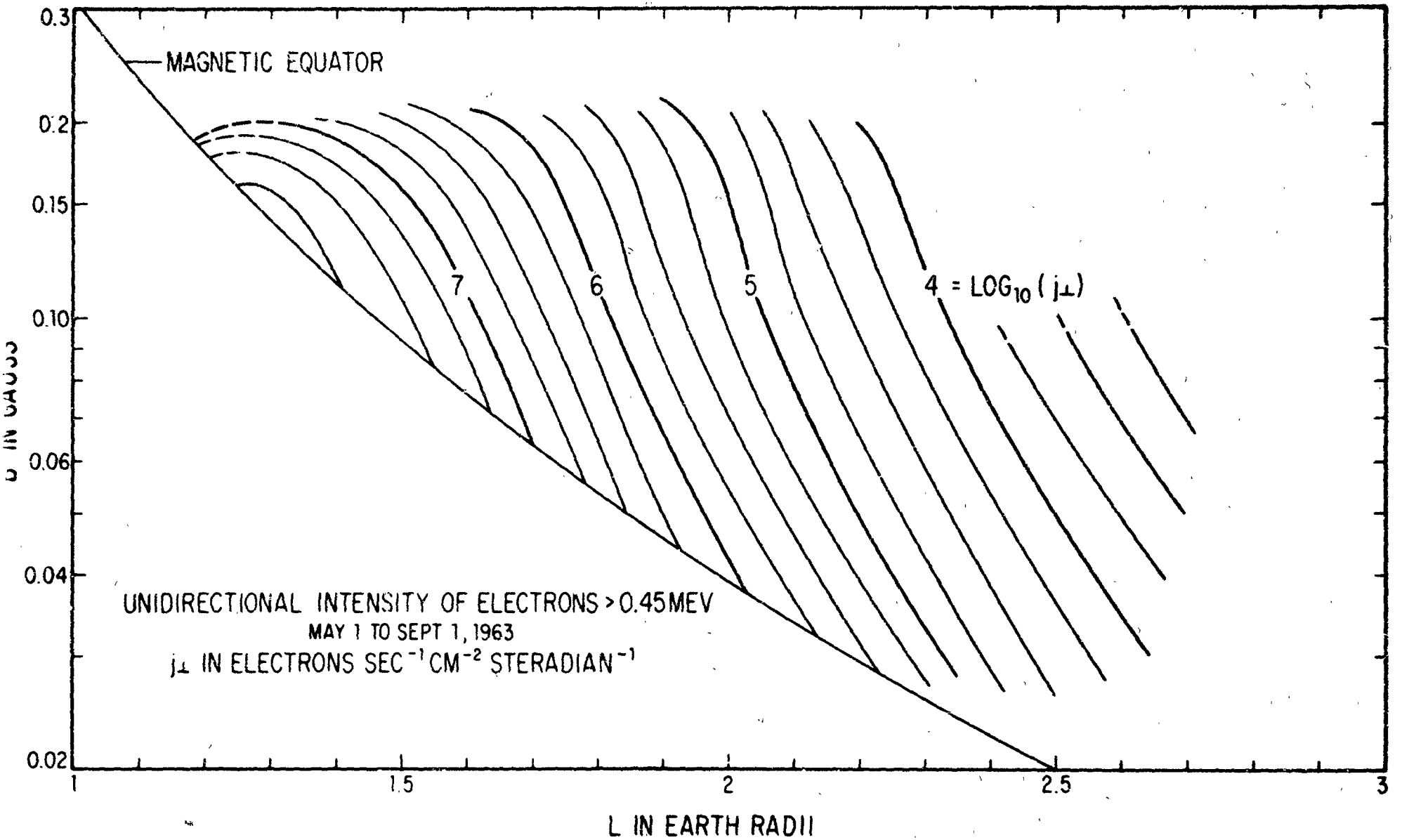
MAGNETIC EQUATOR
7
6
5
4 = LOG10 (j⊥)
UNIDIRECTIONAL INTENSITY OF ELECTRONS > 0.45MEV
MAY 1 TO SEPT 1, 1963
j⊥ IN ELECTRONS SEC-1 CM-2 STERADIAN-1
0.3
0.2
0.15
0.10
0.06
0.04
0.02
1
1.5
2
2.5
3
L IN EARTH RADII

Figure 12

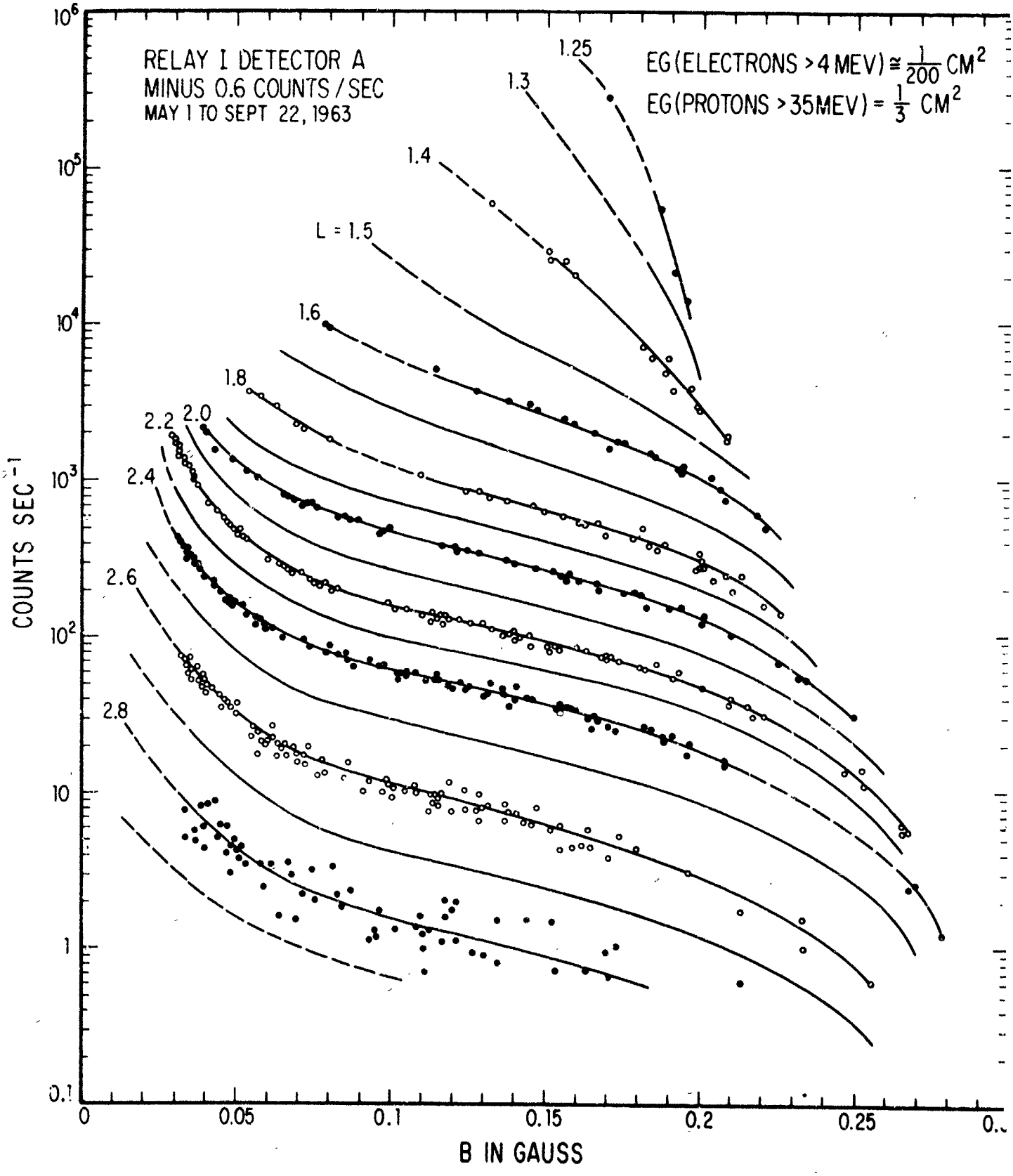
RELAY I DETECTOR A
MINUS 0.6 COUNTS / SEC
MAY 1 TO SEPT 22, 1963
EG(ELECTRONS > 4 MEV) ≅ 1/200 CM²
EG(PROTONS > 35MEV) = 1/3 CM²
1.25
1.3
1.4
L = 1.5
1.6
1.8
2.0
2.2
2.4
2.6
2.8
COUNTS SEC⁻¹
B IN GAUSS
10⁶
10⁵
10⁴
10³
10²
10
1
0.1
0
0.05
0.1
0.15
0.2
0.25

Figure 13

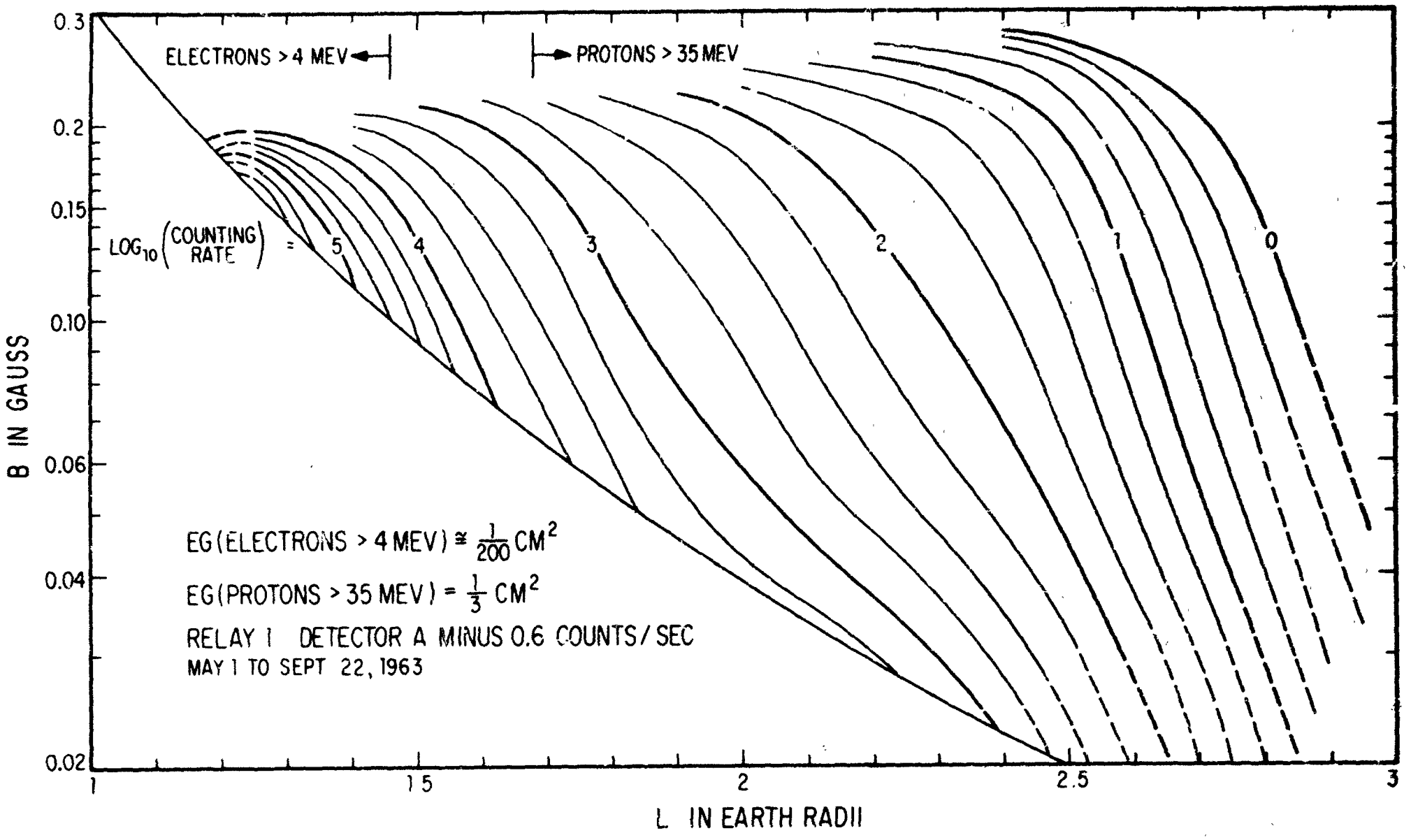
ELECTRONS > 4 MEV
PROTONS > 35 MEV
LOG10 (COUNTING RATE) =
5
4
3
2
1
0
EG(ELECTRONS > 4 MEV) ≅ 1/200 CM2
EG(PROTONS > 35 MEV) = 1/3 CM2
RELAY I DETECTOR A MINUS 0.6 COUNTS/SEC
MAY 1 TO SEPT 22, 1963
B IN GAUSS
0.3
0.2
0.15
0.10
0.06
0.04
0.02
1
1.5
2
2.5
3
L IN EARTH RADII

Figure 14

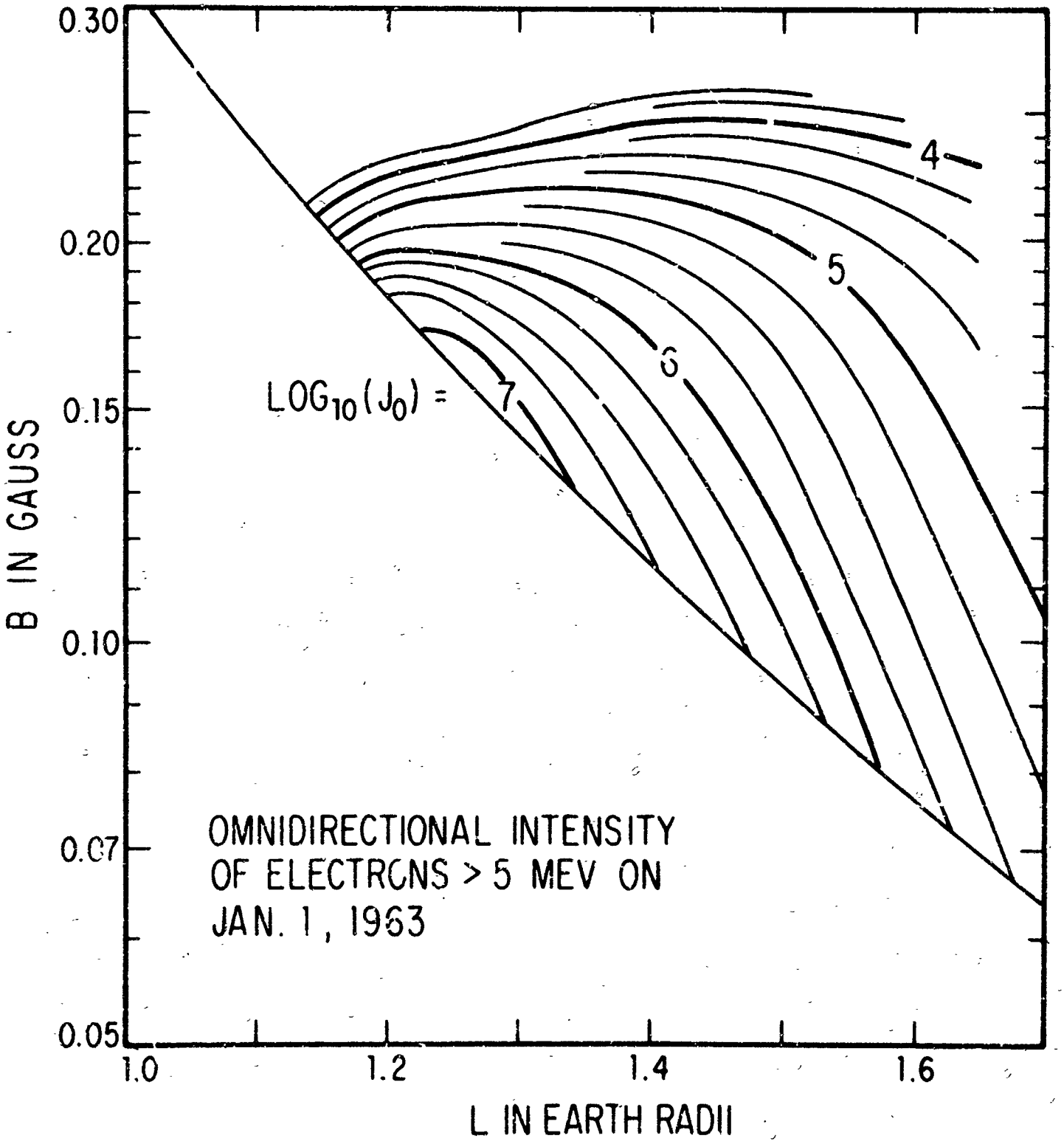
0.30
0.20
0.15
0.10
0.07
0.05
B IN GAUSS
LOG10(J0) =
4
5
6
7
OMNIDIRECTIONAL INTENSITY
OF ELECTRONS > 5 MEV ON
JAN. 1, 1963
1.0
1.2
1.4
1.6
L IN EARTH RADII

Figure 15

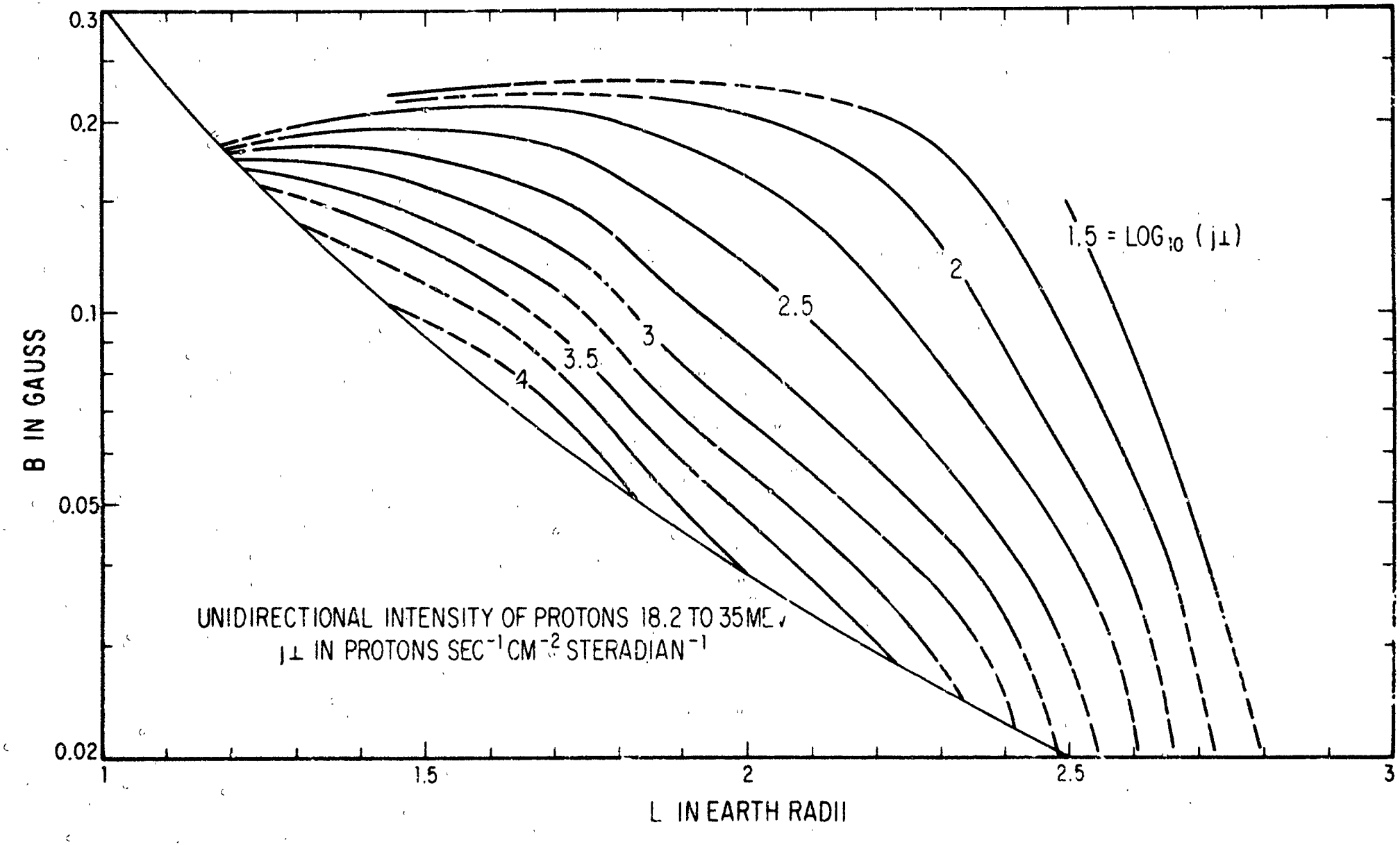
0.3
0.2
0.1
0.05
0.02
B IN GAUSS
1
1.5
2
2.5
3
L IN EARTH RADII
1.5 = LOG10 (j⊥)
2
2.5
3
3.5
4
UNIDIRECTIONAL INTENSITY OF PROTONS 18.2 TO 35MEV
j⊥ IN PROTONS SEC-1 CM-2 STERADIAN-1

Figure 16

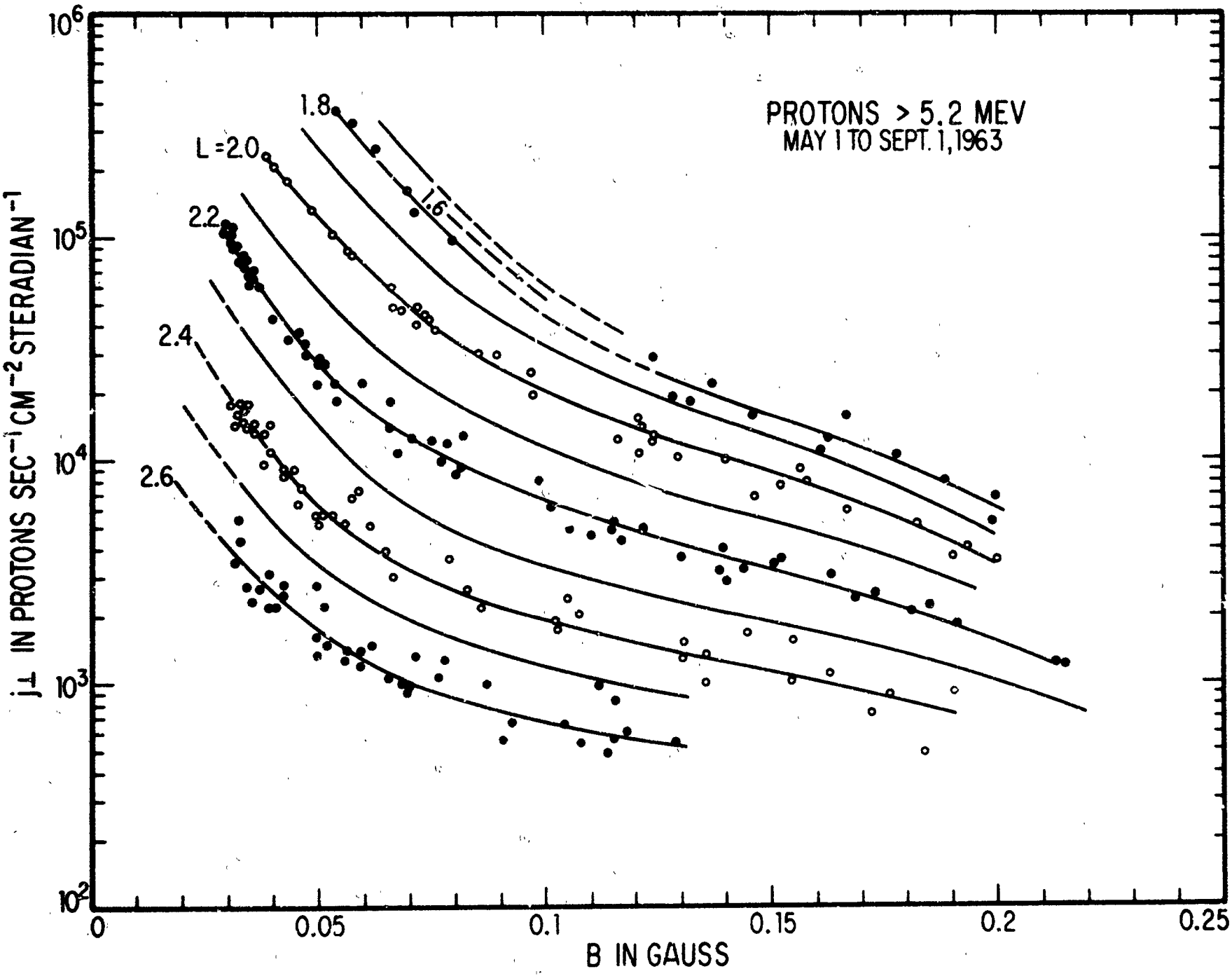
PROTONS > 5.2 MEV
MAY 1 TO SEPT. 1, 1963
L = 2.0
1.8
1.6
2.2
2.4
2.6
10^6
10^5
10^4
10^3
10^2
$j_\perp$ IN PROTONS $SEC^{-1} CM^{-2} STERADIAN^{-1}$
0
0.05
0.1
0.15
0.2
0.25
B IN GAUSS

Figure 17

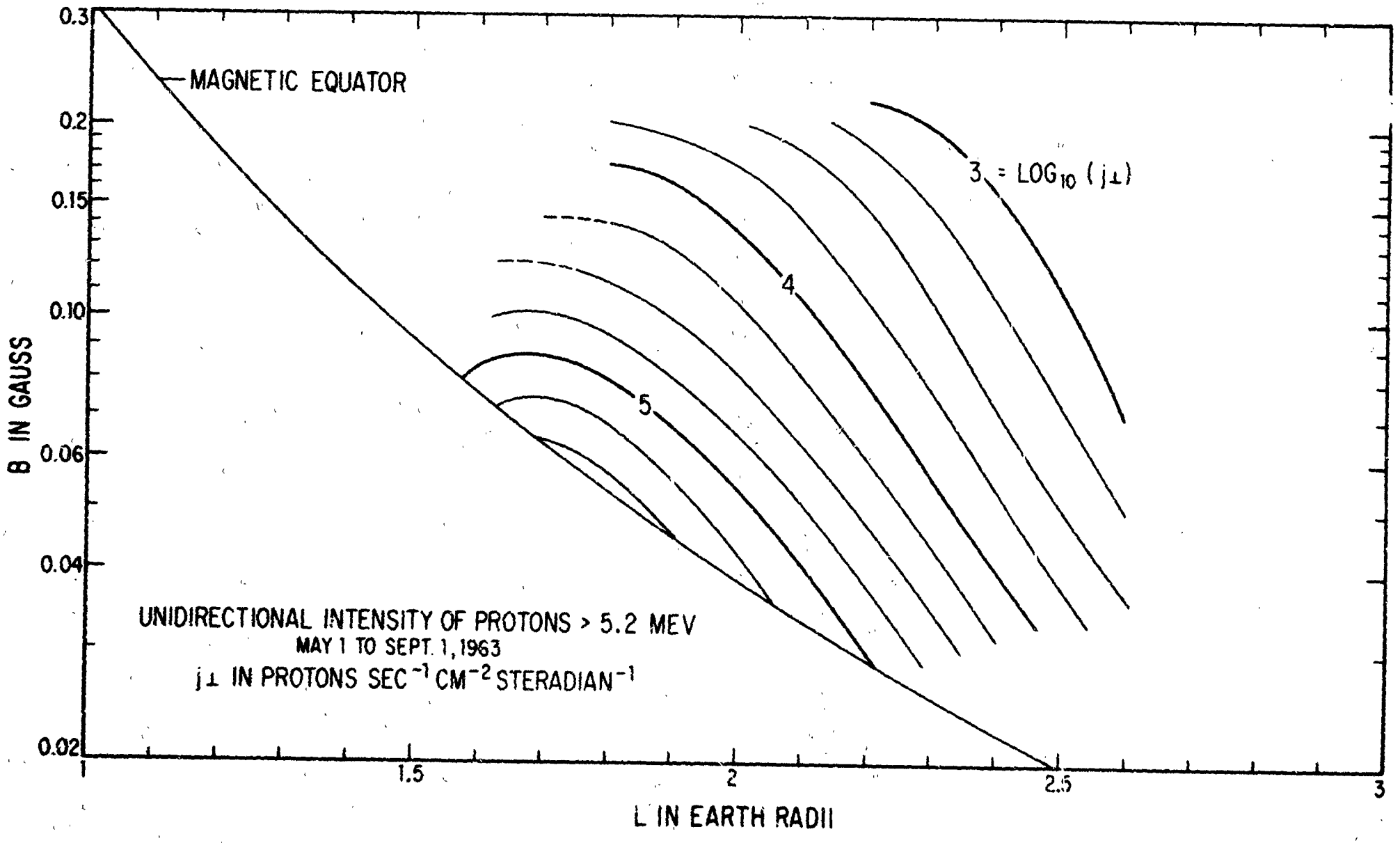
MAGNETIC EQUATOR
3 = LOG10 (j⊥)
4
5
UNIDIRECTIONAL INTENSITY OF PROTONS > 5.2 MEV
MAY 1 TO SEPT. 1, 1963
j⊥ IN PROTONS SEC-1 CM-2 STERADIAN-1
B IN GAUSS
0.3
0.2
0.15
0.10
0.06
0.04
0.02
1
1.5
2
2.5
3
L IN EARTH RADII

Figure 18

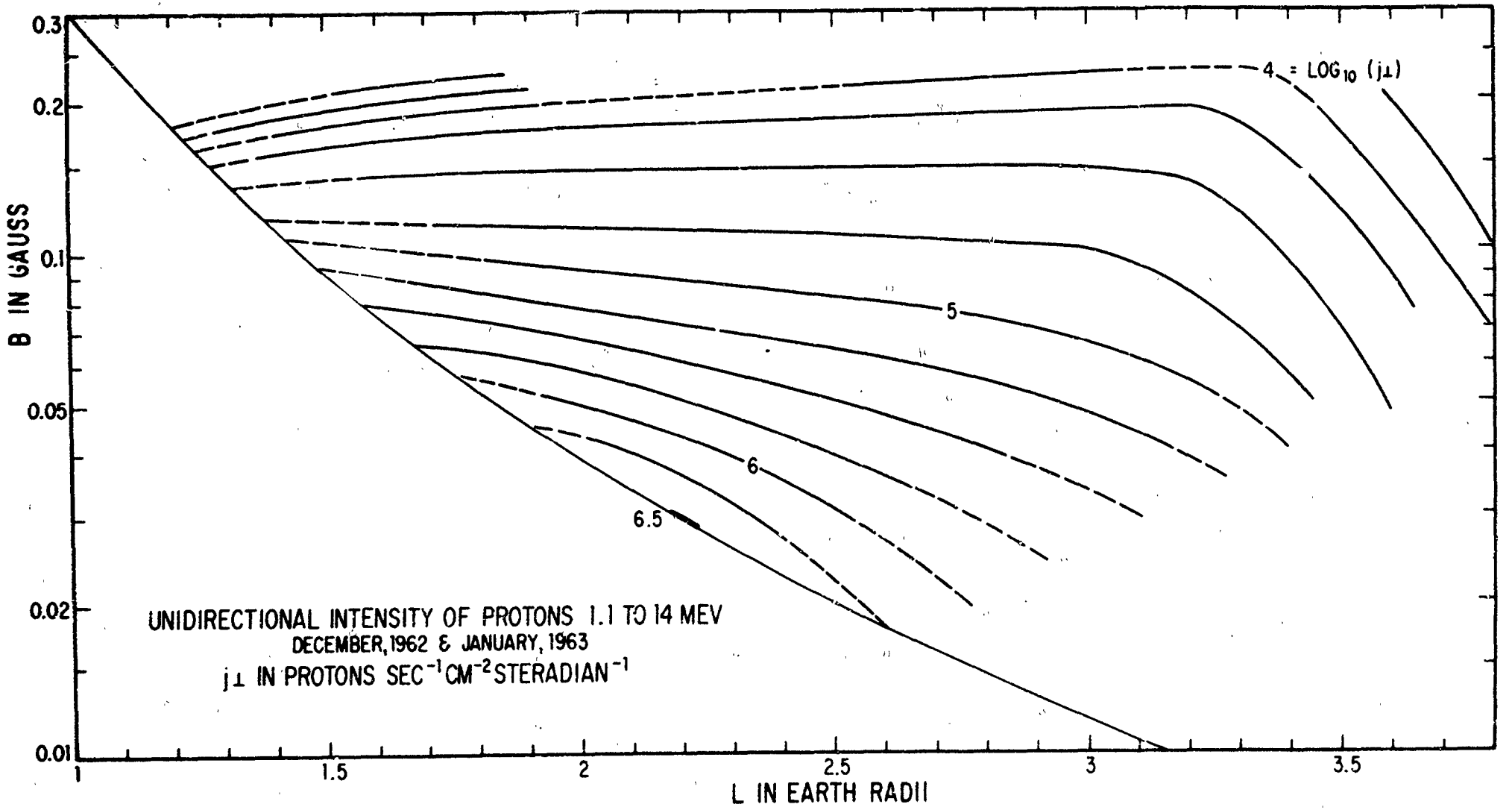
0.3
0.2
0.1
0.05
0.02
0.01
B IN GAUSS
4 = LOG10 (j⊥)
5
6
6.5
UNIDIRECTIONAL INTENSITY OF PROTONS 1.1 TO 14 MEV
DECEMBER, 1962 & JANUARY, 1963
j⊥ IN PROTONS SEC-1 CM-2 STERADIAN-1
1
1.5
2
2.5
3
3.5
L IN EARTH RADII

Figure 19

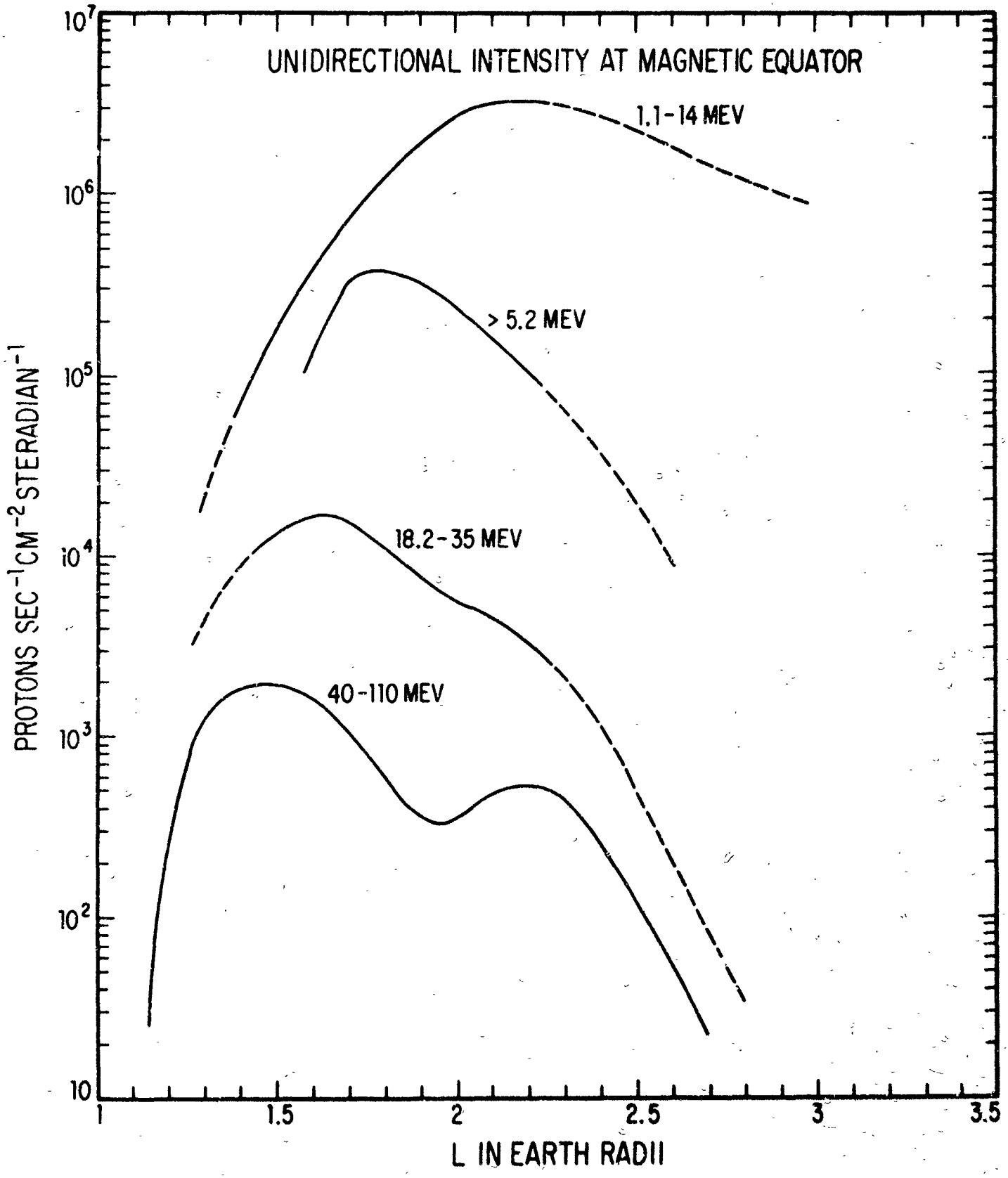
UNIDIRECTIONAL INTENSITY AT MAGNETIC EQUATOR
1.1-14 MEV
> 5.2 MEV
18.2-35 MEV
40-110 MEV
PROTONS SEC^{-1}CM^{-2}STERADIAN^{-1}
10^7
10^6
10^5
10^4
10^3
10^2
10
1
1.5
2
2.5
3
3.5
L IN EARTH RADII

Figure 20

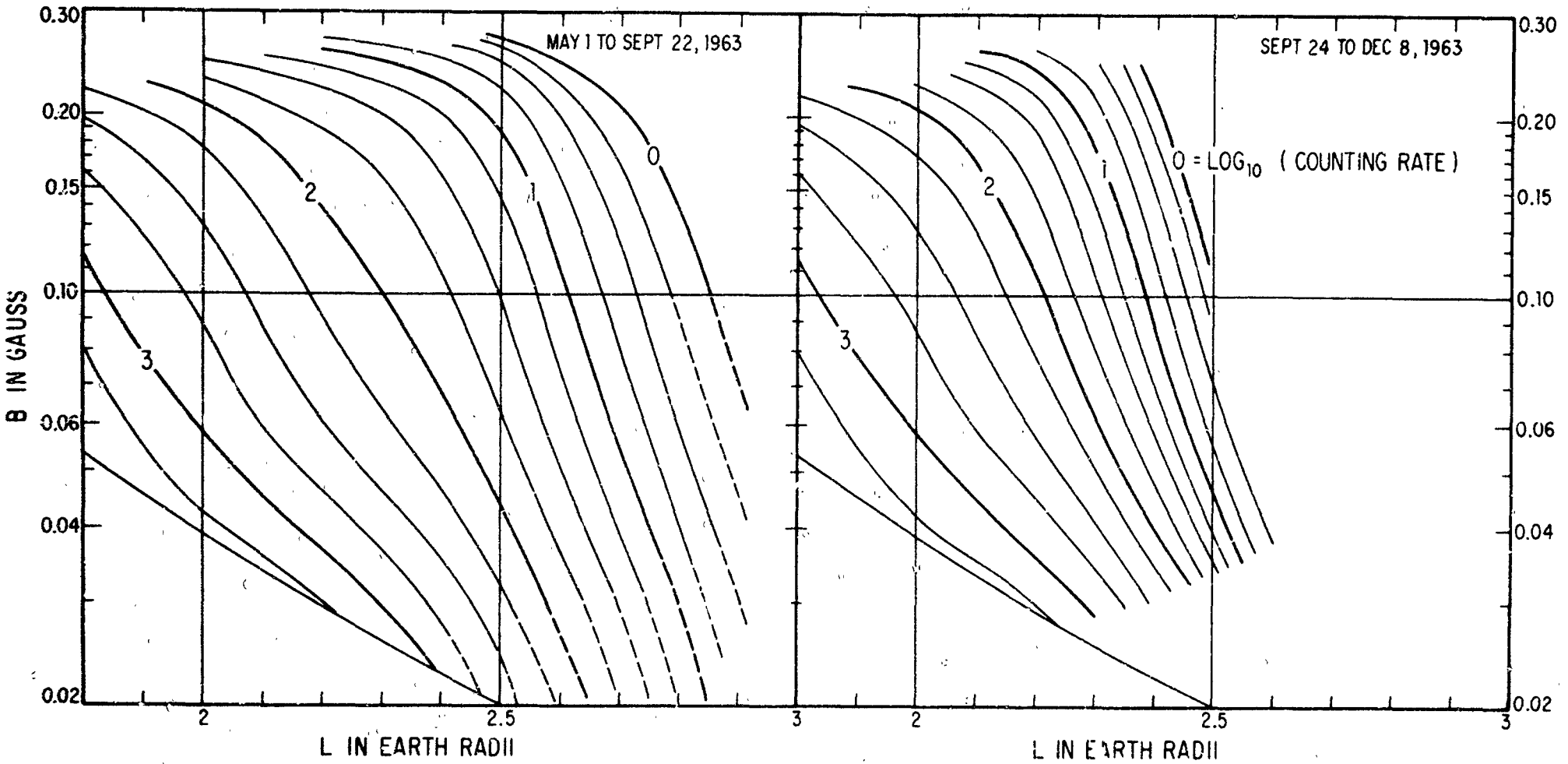
MAY 1 TO SEPT 22, 1963
SEPT 24 TO DEC 8, 1963
0 = LOG10 (COUNTING RATE)
B IN GAUSS
L IN EARTH RADII
L IN EARTH RADII
0.30
0.20
0.15
0.10
0.06
0.04
0.02
2
2.5
3
0
1
2
3

Figure 21

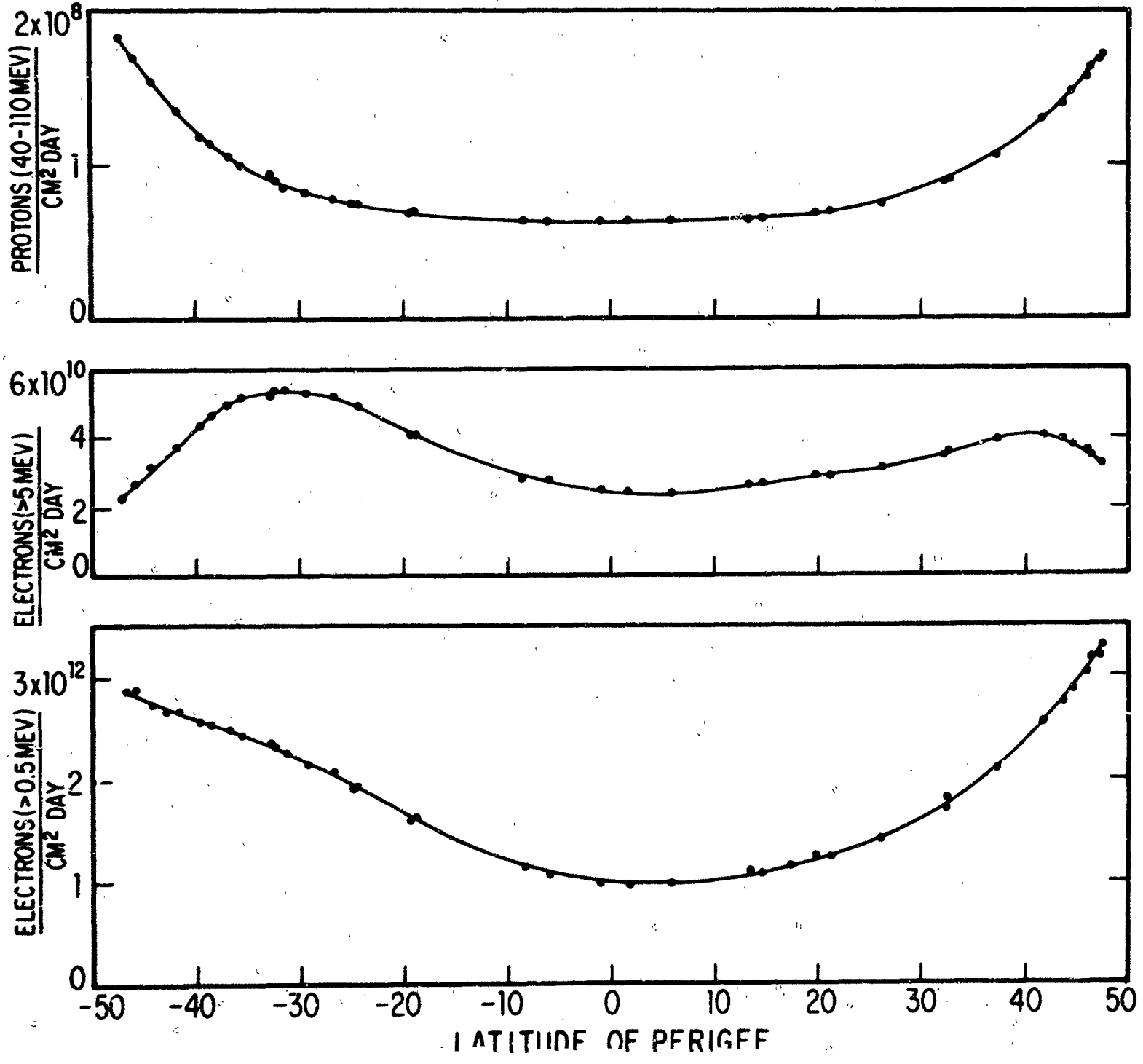
PROTONS (40-110 MEV) / CM² DAY
2x10⁸
1
0
ELECTRONS (>5 MEV) / CM² DAY
6x10¹⁰
4
2
0
ELECTRONS (>0.5 MEV) / CM² DAY
3x10¹²
2
1
0
-50
-40
-30
-20
-10
0
10
20
30
40
50
LATITUDE OF PERIGEE

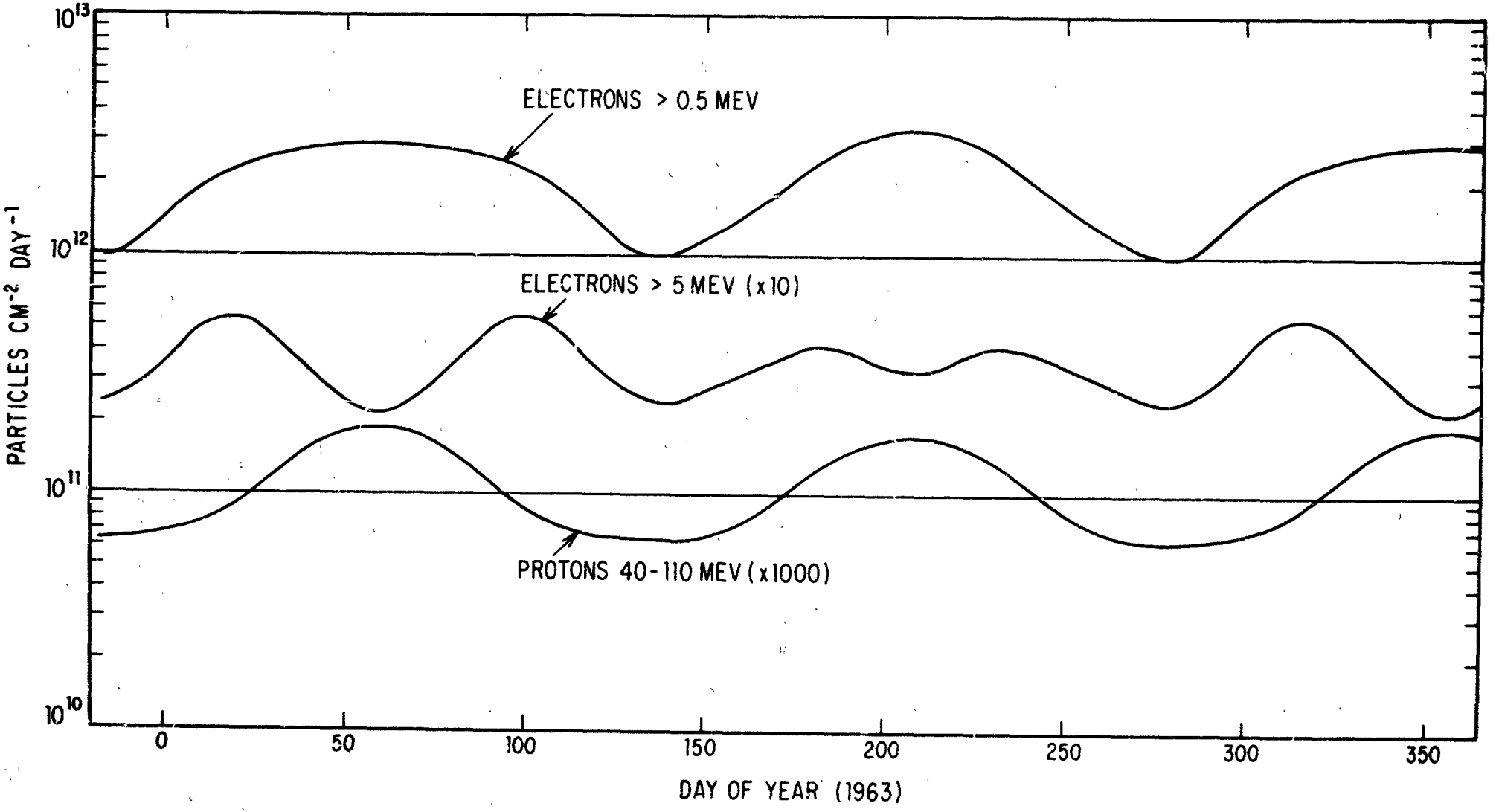
ELECTRONS > 0.5 MEV
ELECTRONS > 5 MEV (x10)
PROTONS 40-110 MEV (x1000)
PARTICLES CM-2 DAY-1
DAY OF YEAR (1963)
10^13
10^12
10^11
10^10
0
50
100
150
200
250
300
350

Figure 23

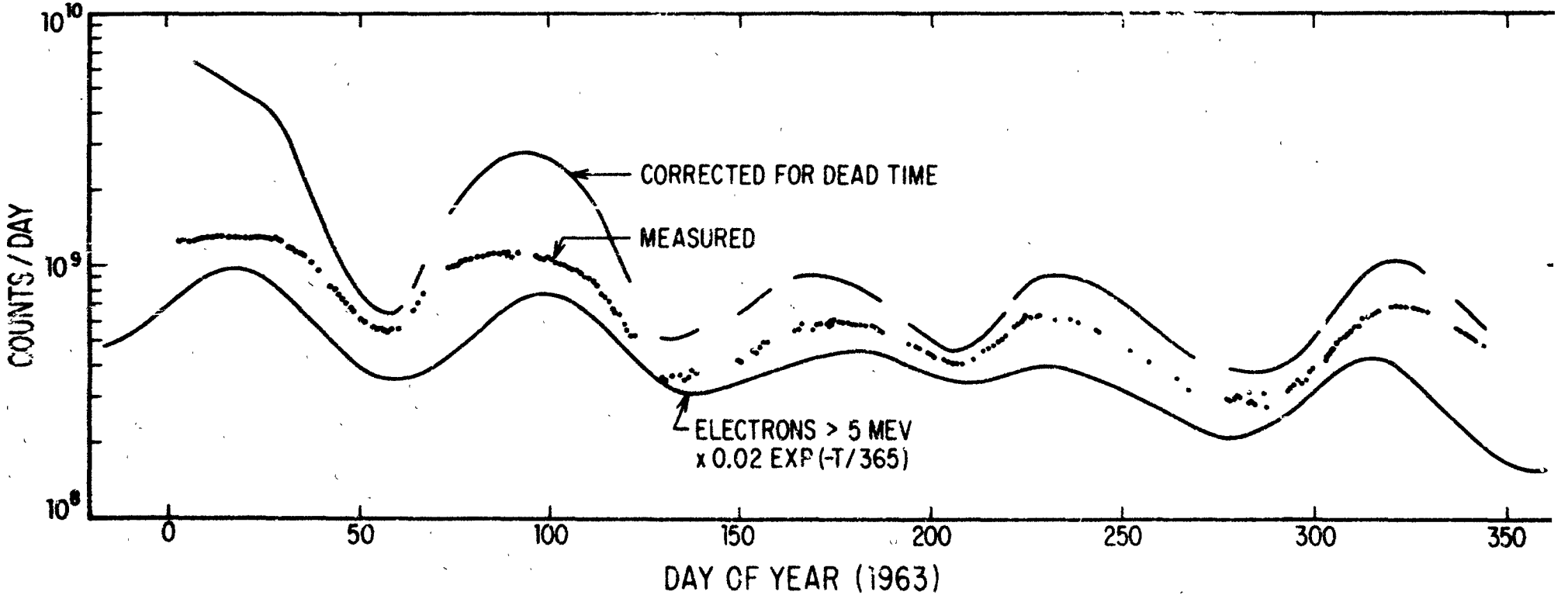
10^{10}
10^{9}
10^{8}
COUNTS / DAY
CORRECTED FOR DEAD TIME
MEASURED
ELECTRONS > 5 MEV
x 0.02 EXP (-T/365)
0
50
100
150
200
250
300
350
DAY OF YEAR (1963)

Figure 24